UCRL-16786

University of California

Ernest O. Lawrence Radiation Laboratory

THE NORMAL MODES OF OSCILLATION OF A UNIFORMLY CHARGED DROP ABOUT ITS SADDLE-POINT SHAPE

TWO-WEEK LOAN COPY

This is a Library Circulating Copy which may be borrowed for two weeks. For a personal retention copy, call Tech. Info. Division, Ext. 5545

DISCLAIMER

This document was prepared as an account of work sponsored by the United States Government. While this document is believed to contain correct information, neither the United States Government nor any agency thereof, nor the Regents of the University of California, nor any of their employees, makes any warranty, express or implied, or assumes any legal responsibility for the accuracy, completeness, or usefulness of any information, apparatus, product, or process disclosed, or represents that its use would not infringe privately owned rights. Reference herein to any specific commercial product, process, or service by its trade name, trademark, manufacturer, or otherwise, does not necessarily constitute or imply its endorsement, recommendation, or favoring by the United States Government or any agency thereof, or the Regents of the University of California. The views and opinions of authors expressed herein do not necessarily state or reflect those of the United States Government or any agency thereof or the Regents of the University of California.

UCRL-16786

UNIVERSITY OF CALIFORNIA

Lawrence Radiation Laboratory
Berkeley, California

AEC Contract No. W-7405-eng-48

THE NORMAL MODES OF OSCILLATION OF A UNIFORMLY CHARGED DROP ABOUT ITS SADDLE-POINT SHAPE

James Rayford Nix

April 1, 1966

THE NORMAL MODES OF OSCILLATION OF A UNIFORMLY CHARGED DROP ABOUT ITS SADDLE-POINT SHAPE

Contents

Abstract v

I. Introduction 1

II. The Drop's Hamiltonian in the Neighborhood of the Saddle Point . 2

A. The Inertia Matrix M 7

1. Determination of M to First Order in 1-x 11

2. Numerical Calculation of M for Arbitrary Values of x . . 14

B. The Stiffness Matrix K 17

1. Determination of K to First Order in 1-x 17

2. Numerical Calculation of K for Arbitrary Values of x . . 19

III. The Normal-Mode Frequencies and Eigenvectors 20

A. Frequencies and Eigenvectors to First Order in 1-x 22

B. Frequencies and Eigenvectors for Arbitrary Values of x . . . 24

IV. Applications and Comparison with Experimental Data 40

A. Transition-State Energy Levels of Collective Oscillations. . 41

B. Probability Distributions for the Saddle-Point States of Motion 42

C. Penetration of the Fission Barrier 44

V. Summary and Conclusion 59

Acknowledgments. 61

Appendices 62

A. The Convergence of the Calculations as a Function of L and N 62

B. The Penetrability of a Cubic Barrier 66

References 69

THE NORMAL MODES OF OSCILLATION OF A UNIFORMLY CHARGED DROP ABOUT ITS SADDLE-POINT SHAPE

James Rayford Nix

Lawrence Radiation Laboratory
University of California
Berkeley, California

April 1, 1966

ABSTRACT

We consider the question of the normal modes of oscillation of an idealized uniformly charged axially symmetric liquid drop about its saddle-point shape and calculate the frequencies and eigenvectors of these modes as functions of the fissility parameter x. Both expansions to first order in 1-x and formulae appropriate for numerical evaluations are derived. For the range $0.7 \leq x \leq 1.0$ numerical results for the 4 lowest symmetric and the 4 lowest asymmetric modes are tabulated at intervals of 0.02 in x for the frequencies, normal-coordinate stiffness and inertia constants, and eigenvectors (with respect to the coefficients α_n in an expansion of the drop's radius vector in Legendre polynomials). For $0.3 \leq x < 0.7$ the results obtained are of limited accuracy, and in this range only graphs of the frequencies of the 3 lowest symmetric modes are included.

Some applications of the results are discussed. These include the transition-state energy levels of collective oscillations, the probability distributions for the saddle-point states of motion, and the penetration of the fission barrier. The formula for the penetrability of a cubic barrier is derived by use of the WKB approximation. The calculated (purely imaginary) frequency for motion in the fission direction, which affects the penetrability of the fission barrier, is compared as a function of x with existing experimental data on fission widths, spontaneous-fission lifetimes and the variation of fission cross sections with excitation energy. The comparison, which is made without the use of any adjustable parameters, indicates that the calculations are capable of reproducing the correct order of magnitude of the fission-direction frequency. The data are at present not sufficiently accurate to provide a sensitive test of the theory.

I. INTRODUCTION

Of fundamental importance in the study of any physical system is the question of small oscillations about the system's positions of equilibrium. In the normal fission process there are three relevant equilibrium positions: (1) the initial either spherical or slightly deformed ground state of the compound nucleus, (2) the intermediate highly deformed saddle point and (3) the final either spherical or slightly deformed ground states of the two fragments at infinity. Both the initial ground state of the compound nucleus and the final ground states of the two fragments at infinity are positions of stable equilibrium. The small oscillations about these spherical or slightly deformed shapes have been extensively studied by expanding the drops' radius vectors in spherical harmonics.

On the other hand, the normal modes of oscillation about the remaining position of equilibrium—the unstable highly deformed saddle-point shape—are more complicated and have not previously been worked out, except for certain of the lower modes in the limit of nearly spherical saddle-point shapes (1,2) or in other approximations (3-5). The present paper considers the normal modes of oscillation of an idealized uniformly charged axially symmetric liquid drop about its saddle-point shape and calculates the frequencies and eigenvectors of these modes as functions of the fissility parameter x. The fissility parameter specifies the relative magnitudes of the Coulomb and surface energies and is defined explicitly by

$$x = \frac{\text{Coulomb energy of sphere}}{2(\text{surface energy of sphere})} \quad .$$

The determination of the saddle-point normal modes is important in the study of the fission process for at least three reasons. First, the quantized energies of these oscillations are of interest in connection with the spectrum of quantum states of a nucleus near its saddle point, i.e. at its transition state. Second, the knowledge of these modes helps determine probability distributions for the states of motion near the saddle point, which can be used as initial conditions for classical dynamical calculations of the division of charged drops. Finally, the (purely imaginary) frequency for unstable motion in the fission direction is related to the probability of penetrating the fission barrier, and consequently to fission

widths, spontaneous-fission lifetimes and the dependence of fission cross sections on excitation energy.

The plan of the paper is as follows: In Section II we discuss the drop's Hamiltonian in the neighborhood of the saddle point, with particular emphasis devoted to the kinetic energy. For both the kinetic and potential energies near the saddle point, expansions to first order in 1-x (i.e. expansions valid for nearly spherical saddle-point shapes) are obtained in addition to formulae appropriate for numerical evaluations. Section III continues with the calculation of the normal-mode frequencies and eigenvectors, including both expansions to first order in 1-x and the results of detailed numerical computations. The three reasons enumerated above for studying the normal modes are discussed as applications of the results in Section IV, which includes a comparison with existing experimental data. The paper is summarized in Section V.

II. THE DROP'S HAMILTONIAN IN THE NEIGHBORHOOD OF THE SADDLE POINT

For the determination of the normal modes of oscillation about a position of equilibrium it is sufficient to calculate the Hamiltonian in the harmonic approximation, i.e. to retain in a Taylor expansion of the kinetic and potential energies about the equilibrium position only terms that are quadratic in the coordinates and velocities (or momenta). Whereas for arbitrary deformations the Hamiltonian of a nucleus undergoing fission depends explicitly upon the particular model that is used, at least the structure of the drop's Hamiltonian in the neighborhood of the saddle point is completely model independent. Because of this, much of what is said in the present paper does not depend upon our specialization to the liquid-drop model: although the numerical results would be somewhat different had another model been employed, the same general procedure could be followed in determining the modes of collective oscillation, and the qualitative considerations concerning them would remain unchanged.

We shall not discuss here the important question of how well the liquid-drop model should be expected to represent the collective motion at the saddle point. Instead we refer the reader to Ref. (3) for some general

comments on the validity of the liquid-drop model for discussing fission, and to Ref. (6) for a discussion of the disappearance of single-particle shell effects with nuclear deformation. The general situation is that detailed agreement should not be expected between theoretical results calculated on the basis of the liquid-drop model and experimental values for a particular nucleus. On the other hand, the liquid-drop model would be expected to represent adequately the average behavior of nuclei throughout the periodic table.

In the liquid-drop model the potential-energy part of the Hamiltonian is simply a sum of surface and Coulomb energies. Once the boundary of the drop is specified the potential energy is uniquely determined and may be calculated in a standard way. On the other hand, the kinetic-energy part of the Hamiltonian is not uniquely determined by specifying the drop's boundary and its time rate of change. One must in addition specify the nature of the hydrodynamic flow of the fluid inside the drop, i.e. the curl (rotation or vorticity) in the system. Thus a thorough treatment of the saddle-point normal modes even within the liquid-drop model would require the study of the system for various types of hydrodynamic flow, consistent with one and the same motion of the boundary. As the natural first step we consider here the case of hydrodynamic flow that is completely irrotational.

The present treatment is restricted to the case of deformations that are axially symmetric. This excludes the possibility of discussing various modes of motion that are of direct physical interest, for example gamma-like vibrations and the bending or "wriggling" of the saddle-point configuration. The restriction to axial symmetry is motivated primarily by computational simplicity—especially the Coulomb energy of a non-axially symmetric drop is far more difficult to evaluate numerically than the corresponding quantity for an axially symmetric drop. However, since the Hamiltonian near the saddle point contains no interaction terms coupling the axially symmetric and non-axially symmetric distortions, the normal modes considered here would be unchanged by the inclusion of non-axially symmetric distortions.

Furthermore there are many phenomena in fission that are not expected to depend significantly upon deviations from axial symmetry. Thus the spectrum of axially symmetric collective states at the saddle point, the

penetration of the fission barrier, and such quantities as the division of mass, the fragments' translational kinetic energies and their excitation energies can all be discussed without recourse to non-axially symmetric distortions. On the other hand, a consideration of non-axially symmetric distortions would be required for a discussion of such phenomena as the spectrum of non-axially symmetric collective states at the saddle point and the angular momenta of the fragments at infinity (which are affected by bending and wriggling vibrations) and should also be included when discussing fragment angular distributions (since bending, wriggling and gamma-like vibrations contribute components of angular momentum along the symmetry axis).

The deformation of the drop is described here by an expansion of the drop's radius vector as a function of angle θ and time t in Legendre polynomials:

$$R(\theta,t) = \frac{1}{\lambda[\underset{\sim}{\alpha}(t)]}\left[1 + \sum_{n=1}^{N} \alpha_n(t)\, P_n(\cos\theta)\right] \quad , \tag{1}$$

where the special choice of N = 18 is made throughout. We adopt a system of natural units in which the radius vector $R(\theta,t)$ is measured in units of the radius R_0 of the initial sphere. The volume-preserving normalization constant $\lambda[\underset{\sim}{\alpha}(t)]$ is given explicitly by (7)

$$\lambda^3 = 1 + \sum_{n=1}^{N} \frac{3}{(2n+1)}\, \alpha_n^{\,2} + \tfrac{1}{2} \sum_{n=1}^{N} \sum_{m=1}^{N} \sum_{\ell=1}^{N} (\ell mn)\, \alpha_\ell \alpha_m \alpha_n \quad , \tag{2}$$

where the coefficients (ℓmn) are the integrals of the product of three Legendre polynomials:

$$(\ell mn) = \int_{-1}^{+1} P_\ell(\mu)\, P_m(\mu)\, P_n(\mu)\, d\mu \quad . \tag{3}$$

With the inclusion of α_1 as one of the N generalized coordinates purely center-of-mass displacements of the drop can be described.

The kinetic and potential energies in the neighborhood of the saddle point are written in the harmonic approximation as

$$\mathcal{T} = \frac{1}{2} \sum_{n=1}^{N} \sum_{m=1}^{N} M_{mn} \dot{\alpha}_m \dot{\alpha}_n$$

and

$$\mathcal{V} - \hat{\mathcal{V}} = \frac{1}{2} \sum_{n=1}^{N} \sum_{m=1}^{N} K_{mn} (\alpha_m - \hat{\alpha}_m)(\alpha_n - \hat{\alpha}_n) \quad .$$

We denote the time derivative of α_m by $\dot{\alpha}_m$ etc. and the saddle-point value of α_m by $\hat{\alpha}_m$ etc. Since the saddle-point shapes are symmetric all $\hat{\alpha}_m$ for odd values of m are zero. We shall discuss later the calculation of the inertia (or effective-mass) matrix M; the elements of the stiffness (or elastic) matrix K are given by

$$K_{mn} = \frac{\widehat{\partial^2 \mathcal{V}}}{\partial\alpha_m \partial\alpha_n} \quad .$$

Because the saddle-point shapes are symmetric it follows that all M_{mn} and all K_{mn} for which m is even and n is odd or vice versa are zero. Thus neither the kinetic nor the potential energies near the saddle point contain interaction terms coupling the symmetric and asymmetric distortions.

The primary reason for our choice of the above parametrization is that in terms of it (with N = 18) the shapes, energies and certain other properties of saddle-point configurations have recently been calculated by Cohen and Swiatecki (8) as functions of the fissility parameter x over the range $0.3 \leq x \leq 1.0$. In fact in terms of this parametrization both the even $\hat{\alpha}_m$ and the matrix K that together define the potential energy in the neighborhood of the saddle point are already known for this range of x. [However, as discussed in Ref. (8) the specification of a saddle point in terms of this parametrization is only moderately successful for $x < 0.7$ and is of uncertain accuracy, at least in some respects, for $x < 0.5$. This difficulty in correctly specifying the saddle point would be expected to lead to inaccuracies in the calculated frequencies and eigenvectors for $x < 0.7$.] Another advantage of this parametrization is that in terms of it (with N arbitrary) both the inertia matrix M and the stiffness matrix K (and hence the frequencies and eigenvectors) can be easily calculated to first order in 1-x.

The coordinate system is of course in general completely arbitrary, provided only that it is capable of adequately describing the deformations under consideration. The results obtained for the frequencies and the actual displacements associated with the normal modes are invariant with respect to such a change of coordinates. On the other hand, the inertia and stiffness matrices and the values of the components of the eigenvectors are not invariant under a change of coordinate system. It is desirable to use a parametrization in which the normal coordinates correspond as closely as possible to the original coordinates. For the coordinate system we have chosen this is the case when x is close to 1 but not for smaller values of x.

For an idealized droplet there are an infinite number of normal modes of oscillation. However, since our parametrization contains only 18 generalized coordinates there appear in our calculation only 18 modes of oscillation. One is interested physically in the lower modes, and it turns out (at least for $x \geq 0.7$, where the saddle-point shapes do not have thin necks) that these modes can be accurately calculated with only 18 coordinates (see Appendix A). Of course our results for the higher modes of oscillation (say in particular the 17th and 18th) will in general be somewhat in error.

In the following subsection we discuss the calculation of the inertia matrix M and in Subsection II.B the stiffness matrix K. Once the inertia and stiffness matrices have been determined the frequencies and eigenvectors of the normal modes can be readily obtained in a standard way.

A. The Inertia Matrix M

We denote by $\underset{\sim}{v} = \underset{\sim}{v}(\underset{\sim}{r},t)$ the velocity of fluid flow inside the drop at position $\underset{\sim}{r} = (r,\theta)$ and time t. (Because we consider only the case of axial symmetry we do not indicate explicitly the dependence of $\underset{\sim}{r}$ upon the azimuthal angle.) Since the hydrodynamic flow is assumed irrotational ($\nabla \times \underset{\sim}{v} = 0$) the velocity vector can be written as the gradient of a velocity potential φ, i.e.

$$\underset{\sim}{v} = \nabla\varphi = \nabla\varphi(\underset{\sim}{r},t) \quad .$$

The fluid is further assumed incompressible; it therefore follows from the equation of continuity that the velocity field $\underset{\sim}{v}$ is solenoidal, i.e.

$$\nabla\cdot\underset{\sim}{v} = \nabla^2\varphi = 0 \quad .$$

The total kinetic energy of the flow of fluid arising from changes in the boundary of the drop is

$$\mathscr{T} = \tfrac{1}{2}\,\rho\int \underset{\sim}{v}^2\, d\tau = \tfrac{1}{2}\,\rho\int (\nabla\varphi)^2\, d\tau \quad ,$$

where ρ denotes the drop's mass density and $d\tau$ an element of volume. In terms of our natural system of units in which masses are measured in units of the total mass M_0 of the drop and distances in units of the radius R_0 of the original spherical drop,

$$\rho = 3/(4\pi) \quad .$$

By use of the vector identity

$$\nabla\cdot(\varphi\nabla\varphi) = (\nabla\varphi)^2 + \varphi\,\nabla^2\varphi \quad ,$$

the relation $\nabla^2\varphi = 0$, and Gauss' divergence theorem to transform from a volume to a surface integral, we obtain for the kinetic energy the usual hydrodynamic result:

$$\mathscr{T} = \frac{1}{2}\,\rho \int \varphi \nabla \varphi \cdot d\underset{\sim}{S} \quad ,$$

where $d\underset{\sim}{S}$ denotes an element of surface area.

It is notationally convenient to introduce the function $F(\underset{\sim}{r},t)$ so that the equation

$$F(\underset{\sim}{r},t) = r - R(\theta,t) = 0 \tag{4}$$

defines the surface of the drop. In terms of this function the element of surface area is

$$d\underset{\sim}{S} = (\nabla F)R^2 \, d\Omega \quad ,$$

where $d\Omega$ denotes an element of solid angle and for an axially symmetric drop becomes simply $2\pi \, d\mu$, where $\mu = \cos\theta$, upon integration over the azimuthal angle.

The kinematical boundary condition is that the total derivative with respect to time of the function F be zero (9),

$$\frac{DF}{Dt} = \nabla F \cdot \dot{\underset{\sim}{r}} + \frac{\partial F}{\partial t} = \nabla F \cdot \nabla \varphi + \frac{\partial F}{\partial t} = 0 \quad . \tag{5}$$

By use of the above results we obtain for the kinetic energy of an idealized axially symmetric drop

$$\mathscr{T} = \frac{1}{2}\left(\frac{3}{2}\right) \int_{-1}^{+1} \varphi \left(-\frac{\partial F}{\partial t}\right) R^2 \, d\mu \quad . \tag{6}$$

From Eqs. (4) and (1) it follows that

$$-\frac{\partial F}{\partial t} = \frac{\partial R}{\partial t} = \frac{1}{\lambda} \sum_{n=1}^{N} \left[P_n - R\left(\frac{\partial \lambda}{\partial \alpha_n}\right)\right] \dot{\alpha}_n \quad , \tag{7}$$

where λ is given by Eq. (2) and where from it we obtain by differentiation

$$\frac{\partial\lambda}{\partial\alpha_n} = \frac{1}{\lambda^2}\left[\frac{2}{(2n+1)}\,\alpha_n + \tfrac{1}{2}\sum_{m=1}^{N}\sum_{\ell=1}^{N}(\ell mn)\,\alpha_\ell\alpha_m\right] \quad . \tag{8}$$

The only unknown quantity appearing in expression (6) for $\mathscr{T}$ is the velocity potential φ. Since φ is a harmonic function that must remain finite at the origin it can be approximated in terms of the known solutions $r^\ell P_\ell$ of Laplace's equation, i.e.

$$\varphi = \sum_{\ell=1}^{L} b_\ell[\underset{\sim}{\alpha}(t),\underset{\sim}{\dot{\alpha}}(t)]\; r^\ell P_\ell(\cos\theta) \quad .$$

Because the velocity $\underset{\sim}{v}$ is obtained from φ by <u>spatial</u> differentiation it follows that the coefficients b_ℓ are linear in the N generalized velocities $\dot{\alpha}_m$. Thus

$$\varphi = \sum_{m=1}^{N}\sum_{\ell=1}^{L} b_\ell^m[\underset{\sim}{\alpha}(t)]\; r^\ell P_\ell(\cos\theta)\,\dot{\alpha}_m \quad , \tag{9}$$

where the unknown coefficients b_ℓ^m are to be determined from the kinematical boundary condition (5).

In general an infinite number of terms would be required in the expansion of φ to represent the velocity potential exactly, even though the number N of generalized coordinates is finite. However, it turns out in practice that as long as L is somewhat greater than N the final results are independent of L to the desired accuracy, at least for $x \geq 0.7$, where the saddle-point shapes do not have thin necks (see Appendix A). For the calculations reported here L was chosen equal to 30.

By substituting Eq. (7) for $\partial F/\partial t$ and Eq. (9) for φ into (6) and interchanging the order of summations we obtain

$$\mathscr{T} = \tfrac{1}{2}\sum_{n=1}^{N}\sum_{m=1}^{N} M_{mn}\,\dot{\alpha}_m\,\dot{\alpha}_n \quad ,$$

where

$$M_{mn} = \frac{3}{2\lambda}\sum_{\ell=1}^{L} b_\ell^m \int_{-1}^{+1} R^{\ell+2}\,P_\ell\left[P_n - R\left(\frac{\partial\lambda}{\partial\alpha_n}\right)\right] d\mu \tag{10}$$

and where R is given by (1), λ by (2) and $\partial\lambda/\partial\alpha_n$ by (8). This is a general result which can be used to calculate the inertia coefficients for any axially symmetric shape that is specified by the N coefficients α_n in the expansion of the drop's radius vector in Legendre polynomials. For our purposes the result is evaluated only for saddle-point shapes.

From Eq. (10) it is not manifestly clear that the inertia matrix is symmetric. The requirement that M in fact be symmetric (10) can be used to establish a relationship involving weighted sums of the coefficients b_ℓ^m, but in practice the relationship is not very useful. On the other hand, the required symmetry of M does provide an important check on the numerical accuracy of the calculated nondiagonal inertia-matrix elements.

The determination of the unknown coefficients b_ℓ^m will now be discussed. Spatial differentiations of Eqs. (4) and (9) give, respectively

$$\nabla F = \underset{\sim}{e}_r - \frac{1}{\lambda r}\sum_{n=1}^{N} \alpha_n\left(\frac{dP_n}{d\theta}\right)\underset{\sim}{e}_\theta$$

and

$$\nabla\varphi = \sum_{m=1}^{N}\sum_{\ell=1}^{L} b_\ell^m\, r^{\ell-1}\left[\ell P_\ell\, \underset{\sim}{e}_r + \left(\frac{dP_\ell}{d\theta}\right)\underset{\sim}{e}_\theta\right]\dot{\alpha}_m \quad .$$

Unit vectors in the radial and θ directions are denoted respectively by $\underset{\sim}{e}_r$ and $\underset{\sim}{e}_\theta$. Substitution of these two results and Eq. (7) for $\partial F/\partial t$ into the kinematical-boundary-condition equation (5) leads to

$$\sum_{m=1}^{N}\sum_{\ell=1}^{L} b_\ell^m R^{\ell-2}\left[\ell\lambda R P_\ell - \left(\frac{dP_\ell}{d\theta}\right)\sum_{n=1}^{N}\alpha_n\left(\frac{dP_n}{d\theta}\right)\right]\dot{\alpha}_m - \sum_{m=1}^{N}\left[P_m - R\left(\frac{\partial\lambda}{\partial\alpha_m}\right)\right]\dot{\alpha}_m = 0.$$

Since this equation must be satisfied for arbitrary motions of the drop's boundary (i.e. for arbitrary values of the $\dot{\alpha}_m$) it is equivalent to the following N equations:

$$\sum_{\ell=1}^{L} R^{\ell-2}\left(\ell\lambda R P_\ell - P_\ell^1\sum_{n=1}^{N}\alpha_n P_n^1\right) b_\ell^m - \left[P_m - R\left(\frac{\partial\lambda}{\partial\alpha_m}\right)\right] = 0 \quad , \quad m = 1, 2, \ldots, N. \quad (11)$$

Use has also been made of the relation $P_\ell^1(\cos\theta) = -\dfrac{dP_\ell(\cos\theta)}{d\theta}$, where P_ℓ^m denotes an associated Legendre polynomial.

When the boundary-condition equations (11) are applied to symmetric shapes the coupling between the terms representing the even and the odd Legendre polynomials disappears, which means that for symmetric shapes if m is even all b_ℓ^m for odd values of ℓ are zero, and if m is odd all b_ℓ^m for even values of ℓ are zero.

1. Determination of M to First Order in 1-x

We now specialize our above results for M_{mn} to the case of saddle-point shapes that differ only slightly from a sphere. Since most of the remaining formulae are evaluated for saddle-point shapes we shall simplify the notation where there should arise no confusion and write α_n rather than $\hat{\alpha}_n$ etc.

To first order in u = 1-x only one of the coefficients α_n that specify a saddle-point shape is nonzero; this coefficient is given by (7, 11-13)

$$\alpha_2 = \frac{7}{3} u \quad .$$

However, for the first part of this subsection we shall retain α_2 rather than u as an independent variable. The other quantities that we need are given to first order in u by

$$\lambda = 1 \quad ,$$

$$R = 1 + \alpha_2 P_2 \quad ,$$

and

$$\frac{\partial\lambda}{\partial\alpha_m} = \frac{2}{5} \alpha_2 \delta_{2m} \quad ,$$

where

$$\delta_{mn} = \begin{cases} 1 \ , \ m = n \\ 0 \ , \ m \neq n \end{cases} \quad .$$

Substitution of the above results into Eq. (11) gives upon simplification

$$\sum_{\ell=1}^{L} \left[\ell P_\ell + (\ell-1)\ell\, \alpha_2 P_2 P_\ell - \alpha_2 P_2^1\, P_\ell^1 \right] b_\ell^m - \left(P_m - \frac{2}{5}\, \alpha_2 P_0\, \delta_{2m} \right) = 0 \quad .$$

This equation is reduced to a linear combination of Legendre polynomials by use of the following rules for the product of two ordinary or associated Legendre polynomials (14,15):

$$P_2 P_\ell = \frac{3(\ell-1)\ell}{2(2\ell-1)(2\ell+1)}\, P_{\ell-2} + \frac{\ell(\ell+1)}{(2\ell-1)(2\ell+3)}\, P_\ell + \frac{3(\ell+1)(\ell+2)}{2(2\ell+1)(2\ell+3)}\, P_{\ell+2}$$

and

$$P_2^1\, P_\ell^1 = \frac{3(\ell-1)\ell(\ell+1)}{(2\ell-1)(2\ell+1)}\, P_{\ell-2} + \frac{3\ell(\ell+1)}{(2\ell-1)(2\ell+3)}\, P_\ell - \frac{3\ell(\ell+1)(\ell+2)}{(2\ell+1)(2\ell+3)}\, P_{\ell+2} \quad .$$

By solving to first order in u (or α_2) the equations that result from equating to zero the coefficients of the individual Legendre polynomials we obtain

$$b_\ell^m = -\frac{7(m-1)(m^2-3m-2)}{2(m-2)(2m-1)(2m+1)}\, u\, \delta_{\ell,m-2} + \frac{1}{m}\left[1 - \frac{7(m+1)(m^2-m-3)}{3(2m-1)(2m+3)}\, u \right] \delta_{\ell m}$$
$$- \frac{7(m+1)^2}{2(2m+1)(2m+3)}\, u\, \delta_{\ell,m+2} \quad .$$

We now substitute this result for b_ℓ^m into Eq. (10) and evaluate the indicated integrations to first order in u; this gives for the inertia-matrix elements the general formula

$$M_{mn} = \frac{3(7)(m-1)(3m-2)}{2(m-2)(2m-3)(2m-1)(2m+1)}\, u\, \delta_{m-2,n} + \frac{3}{m(2m+1)}\left[1 + \frac{7(m+1)^2}{(2m-1)(2m+3)}\, u \right] \delta_{mn}$$
$$+ \frac{3(7)(m+1)(3m+4)}{2m(2m+1)(2m+3)(2m+5)}\, u\, \delta_{m+2,n} \quad , \tag{12}$$

in natural units of $M_0 R_0^2$. Evaluation of this result for the lower Legendre-polynomial distortions yields

$$M^{sym} = \begin{pmatrix} M_{22} & M_{24} & M_{26} & \cdots \\ M_{42} & M_{44} & M_{46} & \cdots \\ M_{62} & M_{64} & M_{66} & \cdots \\ \vdots & \vdots & \vdots & \end{pmatrix} = \begin{pmatrix} \frac{3}{10}(1+3u) & \frac{1}{2}u & 0 & \cdots \\ \frac{1}{2}u & \frac{1}{12}(1+\frac{25}{11}u) & \frac{70}{429}u & \cdots \\ 0 & \frac{70}{429}u & \frac{1}{26}(1+\frac{343}{165}u) & \cdots \\ \vdots & \vdots & \vdots & \end{pmatrix}$$

and

$$M^{asym} = \begin{pmatrix} M_{11} & M_{13} & M_{15} & \cdots \\ M_{31} & M_{33} & M_{35} & \cdots \\ M_{51} & M_{53} & M_{55} & \cdots \\ \vdots & \vdots & \vdots & \end{pmatrix} = \begin{pmatrix} 1+\frac{28}{5}u & \frac{7}{5}u & 0 & \cdots \\ \frac{7}{5}u & \frac{1}{7}(1+\frac{112}{45}u) & \frac{26}{99}u & \cdots \\ 0 & \frac{26}{99}u & \frac{3}{55}(1+\frac{28}{13}u) & \cdots \\ \vdots & \vdots & \vdots & \end{pmatrix} .$$

The above result for M_{22} has been derived previously in Ref. (15); if comparing formulae it should be noted that although the coefficients in the radius-vector expansion are defined differently there, the difference is unimportant to first order in u. In Ref. (16) the result for M_{22} is given incorrectly.

It is seen that the diagonal inertia-matrix elements are of order u^0 and that the elements adjacent to the diagonal are of order u^1. This result generalizes to the statement that the elements of M^{sym} and M^{asym} situated n positions from the diagonal have leading terms of order u^n.

2. Numerical Calculation of M for Arbitrary Values of x

For arbitrary distortions there are no easy solutions to Eqs. (11) for the coefficients b_ℓ^m. Furthermore for a finite value of L it is in general impossible to satisfy Eqs. (11) exactly. In such cases there are three schemes by which the coefficients b_ℓ^m can be determined so that Eqs. (11) are satisfied approximately [see for example Ref. (17)]. The first is the method of collocation, in which the coefficients are chosen so that Eqs. (11) are exact at L specified points on the drop's surface (say equally spaced in μ). The second is the method of least squares, in which the coefficients are selected so as to minimize the integrals over the drop's surface of the squares of the deviations of Eqs. (11) from zero. The third is Galerkin's weighting-function method, where the coefficients are determined by multiplying Eqs. (11) by L linearly independent weighting functions and integrating over the drop's surface. If the weighting functions are chosen to be the first L Legendre polynomials P_0, P_1, ..., P_{L-1}, then this method is equivalent to requiring that the deviations from zero of Eqs. (11) contain no harmonic components of order less than L.

Test calculations with each of the above three schemes were performed, and all three were satisfactory when x was not too far below 1. However, as functions of decreasing x the inertia matrices calculated by collocation and by Galerkin's weighting-function method became asymmetric (and consequently incorrect) much more rapidly than those calculated by least squares. Therefore the latter method was used for the actual calculations.

The coefficients b_ℓ^m are consequently chosen to minimize the functions

$$f_m(b_1^m, b_2^m, \ldots, b_L^m) = \int_{-1}^{+1} \left\{ \sum_{\ell=1}^{L} R^{\ell-2} \left(\ell\lambda R P_\ell - P_\ell^1 \sum_{n=1}^{N} \alpha_n P_n^1 \right) b_\ell^m - \left[P_m - R\left(\frac{\partial\lambda}{\partial\alpha_m}\right)\right]\right\}^2 d\mu,$$

$$m = 1, 2, \ldots, N \quad ,$$

which would be identically zero if the boundary-condition equations (11) were satisfied exactly. The requirements that the functions f_m be minimum are

$$\frac{\partial f_m}{\partial b_k^m} = 0 \quad , \qquad k = 1, 2, \ldots, L \quad , \qquad m = 1, 2, \ldots, N \quad ,$$

which lead to the systems of equations

$$\sum_{\ell=1}^{L} A_{k\ell}\, b_\ell^m = C_k^m \quad , \qquad k = 1, 2, \ldots, L \quad , \qquad m = 1, 2, \ldots, N, \quad (13)$$

where

$$A_{k\ell} = \int_{-1}^{+1} \left[R^{k-2} \left(k\lambda R P_k - P_k^1 \sum_{n=1}^{N} \alpha_n P_n^1 \right) \right] \left[R^{\ell-2} \left(\ell\lambda R P_\ell - P_\ell^1 \sum_{n=1}^{N} \alpha_n P_n^1 \right) \right] d\mu$$

and

$$C_k^m = \int_{-1}^{+1} \left[R^{k-2} \left(k\lambda R P_k - P_k^1 \sum_{n=1}^{N} \alpha_n P_n^1 \right) \right] \left[P_m - R \left(\frac{\partial \lambda}{\partial \alpha_m} \right) \right] d\mu \quad .$$

The quantities $A_{k\ell}$ and C_k^m were evaluated numerically with 96-point Gaussian quadrature formulae (18). The systems of equations (13) were then solved by use of a Gaussian-elimination method to yield the coefficients b_ℓ^m. After the coefficients b_ℓ^m were determined the elements of the inertia matrix were obtained by evaluating Eq. (10) with a 96-point Gaussian-quadrature formula.

In this way an attempt was made to calculate the inertia matrix M for the saddle-point configurations over the entire range $0.3 \leq x \leq 1.0$ for which saddle points are known in a Legendre-polynomial parametrization. The results obtained are highly accurate in the range $0.7 \leq x \leq 1.0$, i.e. for the Bohr-Wheeler family of saddle-point shapes (8,13). However, as x was decreased below 0.7 there occurred a very rapid loss in accuracy of the numerical procedures employed, particularly as regards the matrix M^{asym} corresponding to asymmetric deformations. For the Frankel-Metropolis family of saddle-point shapes (8,13), i.e. for $x < 0.7$, the calculated values of M^{asym} are in serious error, and those of M^{sym} are somewhat doubtful.

The transition from high numerical accuracy for $x \geq 0.7$ to low accuracy for $x < 0.7$ is related to the fairly rapid change in the properties of saddle-point shapes at $x \approx 0.67$. This change is as follows: For $x \gtrsim 0.67$

saddle-point shapes are cylinder-like with large necks and may be well specified by the first few terms in an expansion of the drop's radius vector in Legendre polynomials. For $x \lesssim 0.67$ the shapes are dumbbell-like with thin necks and require many terms in a radius-vector expansion for their specification (8).

The thin necks and the fairly large number of important α_n coefficients required for $x < 0.7$ have the following effects on the accuracy. In the expansion (9) of the velocity potential most of the individual coefficients b_ℓ^m become comparable in magnitude but of alternating sign so that the velocity potential and finally the inertia-matrix elements themselves are determined as the differences of many very large individual terms. Furthermore the matrix A of Eq. (13) becomes extremely ill-conditioned and is influenced greatly by roundoff errors. This is to be contrasted with the situation when $x > 0.7$, where only a few of the coefficients b_ℓ^m are important and can be accurately determined.

However, the presence of a thin neck affects asymmetric distortions much more than symmetric ones, since the former involve a flow of mass through the neck whereas the latter do not. For this reason the calculated values of M^{sym} are still somewhat reliable even for $x < 0.7$ even though the values of M^{asym} are in serious error.

B. The Stiffness Matrix K

From the inertia matrix we now turn our attention to the stiffness matrix K. In the following subsection we discuss the determination of K to first order in 1-x and in the subsequent subsection the numerical evaluation of K by Cohen and Swiatecki.

1. Determination of K to First Order in 1-x

To first order in u = 1-x the stiffness matrix K can be obtained by performing straightforward differentiations of the known expansions of the surface and Coulomb energies in terms of the Legendre-polynomial coefficients α_n. The potential energy of the drop relative to the potential energy of the initial sphere is given in units of the surface energy of the initial sphere $E_s^{(0)}$ by

$$\mathcal{V} = (B_s - 1) + 2\,x\,(B_c - 1) \quad ,$$

where (7,12,19)

$$B_s = 1 + \tfrac{1}{2} \sum_{n=1}^{N} \frac{(n-1)(n+2)}{(2n+1)} \alpha_n^{\,2} - \frac{1}{3} \sum_{n=1}^{N} \sum_{m=1}^{N} \sum_{\ell=1}^{N} (\ell mn)\, \alpha_\ell \alpha_m \alpha_n + \ldots$$

and

$$B_c = 1 - 5 \sum_{n=1}^{N} \frac{(n-1)}{(2n+1)^2} \alpha_n^{\,2} - \frac{5}{12} \sum_{n=1}^{N} \sum_{m=1}^{N} \sum_{\ell=1}^{N} \frac{(7n-10)}{(2n+1)} (\ell mn)\, \alpha_\ell \alpha_m \alpha_n + \ldots \quad ;$$

the coefficients (ℓmn) are defined by (3). [If comparing with the formulae of Ref. (19) note that the coefficients α_n used there are defined differently and that the coefficient α_1 has been eliminated by conserving the position of the drop's center of mass.]

The elements of the stiffness matrix are calculated by performing second partial differentiations of the potential energy $\mathcal{V}$ with respect to the coordinates α_n and evaluating the resulting derivatives at the saddle point. We find to first order in u that

$$K_{mn} = -\frac{2(3)(5)(7)(m-1)m^2(2m-5)}{(2m-3)^2(2m-1)(2m+1)^2}\, u\, \delta_{m-2,n} + \left[\frac{(m-2)(m-1)(2m+9)}{(2m+1)^2} - \frac{(2)^2(3)(5)(m-1)(m^2+m+1)}{(2m-1)(2m+1)^2(2m+3)}\, u\right] \delta_{mn} - \frac{2(3)(5)(7)(m+1)(m+2)^2(2m-1)}{(2m+1)^2(2m+3)(2m+5)^2}\, u\, \delta_{m+2,n} \quad , \tag{14}$$

in natural units of $E_s^{(0)}$. Evaluation of this formula for the lower Legendre-polynomial distortions gives, in notation analogous to that used for M^{sym} and M^{asym},

$$K^{sym} = \begin{pmatrix} 0 & -\frac{4}{5}u & -\frac{32}{15}u & 0 & \cdots \\ -\frac{32}{15}u & \frac{34}{27} - \frac{20}{33}u & -\frac{9800}{5577}u & & \cdots \\ 0 & -\frac{9800}{5577}u & \frac{420}{169} - \frac{860}{1859}u & & \cdots \\ \vdots & \vdots & \vdots & & \end{pmatrix}$$

and

$$K^{asym} = \begin{pmatrix} 0 + 0u & -\frac{12}{7}u & 0 & \cdots \\ -\frac{12}{7}u & \frac{30}{49} - \frac{104}{147}u & -\frac{5000}{2541}u & \cdots \\ 0 & -\frac{5000}{2541}u & \frac{228}{121} - \frac{2480}{4719}u & \cdots \\ \vdots & \vdots & \vdots & \end{pmatrix} .$$

As was true with the inertia matrices, the elements of K^{sym} and K^{asym} situated n positions from the diagonal have leading terms of order u^n.

2. Numerical Calculation of K for Arbitrary Values of x

As mentioned earlier the stiffness matrix K has already been calculated as a function of x by Cohen and Swiatecki in connection with their determination of saddle-point shapes (8). For a given value of x the stiffness matrix was obtained numerically by fitting a quadratic expression in the α_n coordinates to values of the potential energy in the neighborhood of the saddle point, which was itself determined by an iterative scheme for locating the extremum in a local quadratic representation of the potential energy. Because of the loss of significant figures arising from the subtractions of the values of the potential energy in the neighborhood of the saddle point the accuracy of a stiffness matrix determined in this way is somewhat limited. The available stiffness matrices are sufficiently accurate to permit the calculation of the final quantities of interest (frequencies, normal-coordinate stiffness and inertia constants, and eigenvectors) to about three figures for the region $0.7 \leq x \leq 1.0$ but are somewhat less accurate for $0.3 \leq x < 0.7$ (where the inertia matrices are also of reduced accuracy).

III. THE NORMAL-MODE FREQUENCIES AND EIGENVECTORS

Once the inertia and stiffness matrices are obtained as discussed above the frequencies and eigenvectors of the normal-mode oscillations are determined in a standard way (20). The homogeneous system of N linear equations

$$(K - \omega^2 M)\, v = 0 \tag{15}$$

possesses a solution if and only if

$$\det (K - \omega^2 M) = 0 \quad . \tag{16}$$

Solution of this equation yields the N frequencies ω_n, $n = 1, 2, \ldots, N$. Then for a given ω_n the corresponding eigenvector $v^{(n)}$ is determined, apart from an arbitrary normalization factor, by solving the reduced inhomogeneous system of N-1 linear equations in N-1 unknowns obtained from (15) by discarding one of the equations and setting one of the elements of $v^{(n)}$ equal to unity. The normalization factor is chosen here so that

$$\sum_{m=1}^{N} \left[v_m^{(n)} \right]^2 = 1 \ , \quad n = 1, 2, \ldots, N \quad . \tag{17}$$

Because of the separation of both the inertia matrix and the stiffness matrix into symmetric and asymmetric components it is not necessary to solve explicitly the above systems of equations. Instead we can solve for the frequencies two uncoupled systems of dimensions N/2 and for the eigenvectors two uncoupled systems of dimensions (N/2) - 1. Thus each eigenvector of the original system has N/2 elements that are identically zero according to the rule $v_m^{(n)} = 0$ if either n is even and m is odd or n is odd and m is even.

The determination of the eigenvectors is equivalent to determining the transformation from the original α_n coordinates to the normal coordinates, which we designate by β_n, $n = 1, 2, \ldots, N$. Explicitly the normal-coordinate transformation is

$$\alpha - \hat{\alpha} = V \beta \quad ,$$

where α denotes the N-dimensional column vector with elements $\alpha_1, \alpha_2, \ldots, \alpha_N$; the vector $\hat{\alpha}$ is defined analogously, and V is the square matrix of dimension N whose columns are the eigenvectors $v^{(1)}, v^{(2)}, \ldots, v^{(N)}$.

The eigenvectors satisfy the orthogonality relations

$$v^{(m)'} K v^{(n)} = K_n \delta_{mn} \tag{18a}$$

and

$$v^{(m)'} M v^{(n)} = M_n \delta_{mn} \quad , \tag{18b}$$

where $v^{(m)'}$ is the (row vector) transpose of the column vector $v^{(m)}$. The quantities K_n and M_n represent respectively the stiffness (elastic) constant and inertia constant (effective mass) corresponding to the nth normal mode. It should be noted that both K_n and M_n depend upon the choice of eigenvector normalization and consequently have only relative meaning. On the other hand, the frequency

$$\omega_n = (K_n/M_n)^{\frac{1}{2}}$$

is of course independent of the normalization.

A. Frequencies and Eigenvectors to First Order in 1-x

The solution to first order in $u = 1-x$ of the determinantal equation (16) for the frequencies is very simple. Since the nondiagonal elements of $(K - \omega^2 M)$ are of highest order u^1 they contribute to the determinant terms of highest order u^2 and are therefore irrelevant as regards the frequencies. Thus solution of (16) to first order in u yields immediately

$$\omega_n^2 = K_{nn}/M_{nn} \quad .$$

Upon substituting (14) for K_{nn} and (12) for M_{nn} and simplifying, we find that

$$\omega_n^2 = \frac{(n-2)(n-1)n(2n+9)}{3(2n+1)} - \frac{(n-1)n(14n^4+63n^3+18n^2-157n-66)}{3(2n-1)(2n+1)(2n+3)} u \quad , \qquad (19)$$

in natural units of $E_s^{(0)}/(M_0 R_0^2)$. Evaluation of this formula for the 6 lowest modes gives

$$\omega_1^2 = 0 + 0u \quad ,$$

$$\omega_2^2 = 0 - \frac{8}{3} u \quad ,$$

$$\omega_3^2 = \frac{30}{7} - \frac{328}{21} u \quad ,$$

$$\omega_4^2 = \frac{136}{9} - \frac{4120}{99} u \quad ,$$

$$\omega_5^2 = \frac{380}{11} - \frac{8320}{99} u \quad ,$$

and

$$\omega_6^2 = \frac{840}{13} - \frac{20928}{143} u \quad .$$

The above result for ω_2^2 has been given previously in Fig. 48 of Ref. (1); however, in the same figure ω_3^2 is presented incorrectly. On the other hand, the result for ω_3^2 is given correctly in Ref. (2).

By solving to first order in u the homogeneous system of linear equations obtained by substituting (19), (14) and (12) into (15) we find

for the eigenvectors

$$v_m^{(n)} = -\frac{7(n-1)n(12n^4+16n^3-13n^2-141n-54)}{(2)^2(2n-1)(2n+1)(12n^3-4n^2-41n-30)}\, u\, \delta_{m,n-2} + 1\, \delta_{mn}$$

$$+ \frac{7(n+1)(n+2)(12n^5+64n^4+91n^3+59n^2+194n+120)}{(2)^2 n(2n+1)(2n+3)(12n^3+68n^2+87n-32)}\, u\, \delta_{m,n+2} \quad .$$

By evaluating this formula for the lower modes and separating the results into symmetric and asymmetric components we find for the transformation to normal coordinates

$$\begin{pmatrix} \alpha_2 - \frac{7}{3}u \\ \alpha_4 \\ \alpha_6 \\ \vdots \end{pmatrix} = \begin{pmatrix} 1 & -\frac{109}{51}u & 0 & \cdots \\ \frac{144}{85}u & 1 & -\frac{77175}{25883}u & \cdots \\ 0 & \frac{26495}{11946}u & 1 & \cdots \\ \vdots & \vdots & \vdots & \end{pmatrix} \begin{pmatrix} \beta_2 \\ \beta_4 \\ \beta_6 \\ \vdots \end{pmatrix}$$

and

$$\begin{pmatrix} \alpha_1 \\ \alpha_3 \\ \alpha_5 \\ \vdots \end{pmatrix} = \begin{pmatrix} 1 & -\frac{9}{5}u & 0 & \cdots \\ \frac{14}{5}u & 1 & -\frac{58912}{23067}u & \cdots \\ 0 & \frac{1310}{699}u & 1 & \cdots \\ \vdots & \vdots & \vdots & \end{pmatrix} \begin{pmatrix} \beta_1 \\ \beta_3 \\ \beta_5 \\ \vdots \end{pmatrix} \quad .$$

It is noted that for the nth normal mode when the coordinate α_n is displaced by an amount of order u^0 the coordinates α_{n-2} and α_{n+2} are displaced by amounts of order u^1; in general the changes in α_{n-2m} and α_{n+2m} are of order u^m. It follows from this and the orthogonality relations (18)

that to first order in u the normal-coordinate stiffness and inertia constants are simply the corresponding diagonal elements of the original stiffness and inertia matrices; thus from Eqs. (14) and (12) we have

$$K_n = \frac{(n-2)(n-1)(2n+9)}{(2n+1)^2} - \frac{(2)^2(3)(5)(n-1)(n^2+n+1)}{(2n-1)(2n+1)^2(2n+3)} u$$

and

$$M_n = \frac{3}{n(2n+1)} \left[1 + \frac{7(n+1)^2}{(2n-1)(2n+3)} u \right] .$$

B. Frequencies and Eigenvectors for Arbitrary Values of x

For arbitrary values of x the determinantal equation (16) for the frequencies was solved by a numerical method in which, for given initial guesses for the frequencies, Newton's method was used to iterate until a specified accuracy was obtained. The initial guesses were determined by extrapolating the results previously calculated for higher values of x. The reduced systems of linear equations for the eigenvectors were then solved by use of a Gaussian-elimination method.

In this way the frequencies and eigenvectors were calculated at intervals of 0.02 in x for the range $0.3 \leq x \leq 1.0$. However, as discussed earlier the accuracy of both the stiffness and the inertia matrices, particularly the asymmetric component M^{asym} of the inertia matrix, is poor for $0.3 \leq x < 0.7$. Hence the accuracy of the calculated frequencies and eigenvectors, particularly the asymmetric ones, is also poor for this range of x. We therefore present here detailed results only for the range $0.7 \leq x \leq 1.0$, where the numerical accuracy is adequate, although graphs of the frequencies of the 3 lowest symmetric modes are also given for $0.3 \leq x < 0.7$. As discussed in Appendix A the calculations for $x \geq 0.7$ have converged sufficiently as regards both the number L of terms retained in the expansion of the velocity potential and the number N of generalized coordinates.

Table I summarizes the properties of the normal-mode oscillations as functions of the fissility parameter for $0.7 \leq x \leq 1.0$. The table consists of 16 subtables, one for each value of x at intervals of 0.02. The format

Table I. Properties of normal-mode oscillations as functions of the fissility parameter x.

x	ω_2^2	ω_4^2	ω_6^2	ω_8^2	ω_1^2	ω_3^2	ω_5^2	ω_7^2
	K_2	K_4	K_6	K_8	K_1	K_3	K_5	K_7
$\hat{\lambda}$	M_2	M_4	M_6	M_8	M_1	M_3	M_5	M_7
$\hat{\alpha}_2$	$v_2^{(2)}$	$v_2^{(4)}$	$v_2^{(6)}$	$v_2^{(8)}$	$v_1^{(1)}$	$v_1^{(3)}$	$v_1^{(5)}$	$v_1^{(7)}$
$\hat{\alpha}_4$	$v_4^{(2)}$	$v_4^{(4)}$	$v_4^{(6)}$	$v_4^{(8)}$	$v_3^{(1)}$	$v_3^{(3)}$	$v_3^{(5)}$	$v_3^{(7)}$
$\hat{\alpha}_6$	$v_6^{(2)}$	$v_6^{(4)}$	$v_6^{(6)}$	$v_6^{(8)}$	$v_5^{(1)}$	$v_5^{(3)}$	$v_5^{(5)}$	$v_5^{(7)}$
$\hat{\alpha}_8$	$v_8^{(2)}$	$v_8^{(4)}$	$v_8^{(6)}$	$v_8^{(8)}$	$v_7^{(1)}$	$v_7^{(3)}$	$v_7^{(5)}$	$v_7^{(7)}$
$\hat{\alpha}_{10}$	$v_{10}^{(2)}$	$v_{10}^{(4)}$	$v_{10}^{(6)}$	$v_{10}^{(8)}$	$v_9^{(1)}$	$v_9^{(3)}$	$v_9^{(5)}$	$v_9^{(7)}$
$\hat{\alpha}_{12}$	$v_{12}^{(2)}$	$v_{12}^{(4)}$	$v_{12}^{(6)}$	$v_{12}^{(8)}$	$v_{11}^{(1)}$	$v_{11}^{(3)}$	$v_{11}^{(5)}$	$v_{11}^{(7)}$
$\hat{\alpha}_{14}$	$v_{14}^{(2)}$	$v_{14}^{(4)}$	$v_{14}^{(6)}$	$v_{14}^{(8)}$	$v_{13}^{(1)}$	$v_{13}^{(3)}$	$v_{13}^{(5)}$	$v_{13}^{(7)}$
$\hat{\alpha}_{16}$	$v_{16}^{(2)}$	$v_{16}^{(4)}$	$v_{16}^{(6)}$	$v_{16}^{(8)}$	$v_{15}^{(1)}$	$v_{15}^{(3)}$	$v_{15}^{(5)}$	$v_{15}^{(7)}$
$\hat{\alpha}_{18}$	$v_{18}^{(2)}$	$v_{18}^{(4)}$	$v_{18}^{(6)}$	$v_{18}^{(8)}$	$v_{17}^{(1)}$	$v_{17}^{(3)}$	$v_{17}^{(5)}$	$v_{17}^{(7)}$
1.00	0.000	15.11	64.62	164.7	0.000	4.286	34.55	107.3
	0.0000	1.259	2.485	3.633	0.000	0.612	1.884	3.067
1.0000	0.300	0.0833	0.0385	0.0221	1.000	0.1429	0.0545	0.0286
0.0000	1.000	0.000	0.000	0.000	1.000	0.000	0.000	0.000
0.0000	0.000	1.000	0.000	0.000	0.000	1.000	0.000	0.000
0.0000	0.000	0.000	1.000	0.000	0.000	0.000	1.000	0.000
0.0000	0.000	0.000	0.000	1.000	0.000	0.000	0.000	1.000
0.0000	0.000	0.000	0.000	0.000	0.000	0.000	0.000	0.000
0.0000	0.000	0.000	0.000	0.000	0.000	0.000	0.000	0.000
0.0000	0.000	0.000	0.000	0.000	0.000	0.000	0.000	0.000
0.0000	0.000	0.000	0.000	0.000	0.000	0.000	0.000	0.000
0.0000	0.000	0.000	0.000	0.000	0.000	0.000	0.000	0.000
0.98	-0.051	14.32	61.68	157.9	0.005	4.032	33.26	103.6
	-0.0163	1.244	2.464	3.610	0.005	0.603	1.886	3.070
1.0004	0.317	0.0868	0.0399	0.0229	1.109	0.1495	0.0567	0.0296
0.0438	0.999	-0.044	0.001	0.000	0.998	-0.034	0.001	0.000
0.0007	0.047	0.998	-0.054	0.002	0.058	0.999	-0.049	0.002
0.0000	0.002	0.038	0.997	-0.074	-0.003	0.038	0.997	-0.068
0.0000	0.002	0.000	0.060	0.995	0.002	-0.003	0.056	0.995
0.0001	0.001	0.000	0.000	0.072	-0.002	0.003	-0.002	0.075
0.0001	0.001	0.000	0.000	0.001	0.003	-0.002	0.005	-0.006
0.0001	0.000	0.000	0.000	-0.001	-0.002	0.003	-0.004	0.005
0.0000	0.001	0.000	0.000	-0.001	0.002	-0.002	0.004	-0.005
-0.0002	0.000	0.000	0.000	0.000	-0.001	0.001	-0.003	0.002

Table I (continued)

0.96	-0.102	13.47	58.47	150.6	0.004	3.690	31.46	98.2
	-0.0342	1.217	2.422	3.560	0.005	0.578	1.853	3.016
1.0017	0.334	0.0904	0.0414	0.0236	1.234	0.1565	0.0589	0.0307
0.0909	0.997	-0.086	0.005	-0.001	0.993	-0.069	0.004	0.000
0.0031	0.082	0.993	-0.112	0.011	0.120	0.995	-0.099	0.009
0.0000	0.002	0.080	0.986	-0.149	0.000	0.076	0.989	-0.134
0.0000	0.003	-0.001	0.121	0.977	0.000	-0.004	0.108	0.981
0.0001	0.002	0.001	0.000	0.149	-0.003	0.002	-0.005	0.142
0.0001	0.002	0.000	0.001	0.004	0.002	-0.001	0.004	-0.001
0.0001	0.001	0.000	0.000	-0.002	-0.002	0.001	-0.004	0.002
0.0000	0.001	-0.001	0.000	-0.002	0.002	-0.001	0.003	-0.004
-0.0002	0.001	0.000	-0.001	0.001	-0.001	0.001	-0.004	0.002
0.94	-0.151	12.60	55.00	142.6	0.003	3.372	29.51	93.0
	-0.0527	1.179	2.350	3.472	0.004	0.550	1.796	2.942
1.0038	0.350	0.0936	0.0427	0.0243	1.362	0.1631	0.0609	0.0316
0.1367	0.993	-0.127	0.012	-0.002	0.983	-0.102	0.008	-0.001
0.0069	0.117	0.985	-0.165	0.023	0.186	0.988	-0.146	0.018
-0.0001	0.001	0.120	0.970	-0.217	0.005	0.113	0.977	-0.195
0.0000	0.002	-0.004	0.177	0.951	0.000	-0.006	0.157	0.959
0.0001	0.001	-0.001	0.000	0.220	-0.002	0.000	-0.005	0.206
0.0001	0.002	0.000	-0.002	0.011	0.002	-0.002	0.001	0.001
0.0001	0.002	-0.001	0.001	-0.006	-0.001	0.002	-0.004	0.002
0.0000	0.001	-0.001	0.000	-0.002	0.002	-0.002	0.002	-0.004
-0.0002	0.001	-0.001	0.000	0.000	-0.001	0.001	-0.003	0.001
0.92	-0.187	11.74	51.66	134.9	0.003	3.060	27.63	87.7
	-0.0681	1.133	2.269	3.366	0.004	0.518	1.731	2.846
1.0068	0.365	0.0965	0.0439	0.0249	1.494	0.1694	0.0627	0.0325
0.1830	0.988	-0.167	0.021	-0.003	0.967	-0.133	0.014	-0.002
0.0124	0.152	0.973	-0.218	0.041	0.255	0.980	-0.192	0.032
-0.0004	0.000	0.162	0.947	-0.283	0.012	0.148	0.959	-0.255
-0.0001	0.001	-0.006	0.236	0.913	-0.002	-0.009	0.207	0.929
0.0001	0.002	-0.002	0.003	0.290	-0.001	-0.001	-0.004	0.266
0.0001	0.002	-0.001	-0.004	0.018	0.001	-0.002	0.001	0.008
0.0001	0.002	0.000	0.000	-0.009	0.000	0.002	-0.003	-0.002
0.0000	0.002	-0.001	0.000	-0.004	0.001	-0.002	0.003	-0.005
-0.0002	0.001	-0.001	0.000	0.001	0.000	0.001	-0.003	0.002
0.90	-0.219	10.87	48.16	126.8	0.002	2.744	25.72	82.1
	-0.0829	1.078	2.164	3.230	0.003	0.482	1.651	2.721
1.0108	0.378	0.0992	0.0449	0.0255	1.626	0.1755	0.0642	0.0332
0.2298	0.983	-0.205	0.032	-0.006	0.944	-0.165	0.021	-0.003
0.0197	0.185	0.957	-0.268	0.062	0.329	0.969	-0.236	0.048
-0.0007	-0.002	0.204	0.918	-0.342	0.024	0.185	0.938	-0.308
-0.0003	-0.001	-0.008	0.290	0.866	-0.005	-0.012	0.254	0.892
0.0001	0.003	-0.006	0.008	0.357	-0.002	-0.005	-0.002	0.325
0.0001	0.002	-0.001	-0.009	0.033	0.001	-0.001	-0.005	0.017
0.0001	0.002	0.000	0.001	-0.015	-0.001	0.002	-0.003	-0.007
0.0000	0.002	-0.001	0.000	-0.004	0.001	-0.001	0.001	-0.003
-0.0002	0.002	-0.001	0.001	0.000	0.000	0.000	-0.003	0.002

Table I (continued)

0.88	-0.238	10.02	44.76	118.7	0.002	2.455	23.76	76.7
	-0.0926	1.017	2.048	3.075	0.003	0.445	1.557	2.586
1.0158	0.390	0.1015	0.0458	0.0259	1.754	0.1812	0.0655	0.0337
0.2777	0.976	-0.243	0.047	-0.010	0.914	-0.195	0.030	-0.005
0.0289	0.219	0.938	-0.315	0.087	0.404	0.955	-0.278	0.067
-0.0012	-0.005	0.246	0.883	-0.395	0.038	0.221	0.911	-0.360
-0.0006	-0.004	-0.010	0.344	0.808	-0.010	-0.014	0.304	0.847
0.0001	0.002	-0.011	0.012	0.424	-0.004	-0.009	-0.001	0.384
0.0002	0.003	-0.002	-0.017	0.051	0.002	-0.001	-0.011	0.030
0.0001	0.002	0.000	-0.002	-0.021	-0.001	0.002	-0.005	-0.014
0.0000	0.002	-0.001	0.000	-0.008	0.001	0.000	0.003	-0.005
-0.0002	0.002	-0.001	0.001	0.000	0.000	0.001	-0.001	0.001
0.86	-0.250	9.17	41.31	110.6	0.001	2.171	21.91	71.3
	-0.0999	0.948	1.916	2.898	0.003	0.405	1.459	2.435
1.0221	0.399	0.1034	0.0464	0.0262	1.870	0.1866	0.0666	0.0341
0.3276	0.967	-0.281	0.063	-0.016	0.872	-0.225	0.041	-0.008
0.0405	0.255	0.914	-0.360	0.116	0.485	0.938	-0.319	0.091
-0.0018	-0.008	0.291	0.840	-0.442	0.061	0.261	0.876	-0.407
-0.0012	-0.009	-0.010	0.399	0.740	-0.016	-0.018	0.355	0.791
0.0000	0.003	-0.018	0.020	0.487	-0.007	-0.016	0.003	0.444
0.0002	0.004	-0.003	-0.024	0.073	0.002	-0.002	-0.019	0.046
0.0001	0.003	0.001	-0.004	-0.030	0.000	0.002	-0.006	-0.023
0.0000	0.003	-0.001	0.002	-0.012	0.001	-0.001	0.002	-0.010
-0.0002	0.002	-0.001	0.003	0.000	0.000	0.001	-0.001	0.002
0.84	-0.258	8.31	37.88	102.2	0.001	1.897	19.99	65.6
	-0.1044	0.871	1.770	2.696	0.002	0.363	1.345	2.258
1.0298	0.405	0.1048	0.0467	0.0264	1.964	0.1914	0.0673	0.0344
0.3798	0.957	-0.318	0.083	-0.023	0.818	-0.255	0.053	-0.013
0.0548	0.290	0.886	-0.403	0.148	0.567	0.918	-0.358	0.116
-0.0026	-0.010	0.337	0.791	-0.481	0.090	0.301	0.839	-0.449
-0.0023	-0.015	-0.009	0.451	0.662	-0.024	-0.020	0.404	0.788
0.0000	0.004	-0.030	0.032	0.544	-0.012	-0.026	0.009	0.499
0.0003	0.004	-0.003	-0.037	0.103	0.001	-0.003	-0.033	0.069
0.0002	0.003	0.002	-0.007	-0.038	0.001	0.003	-0.008	-0.032
0.0000	0.003	-0.001	0.003	-0.019	0.002	0.000	0.004	-0.013
-0.0002	0.003	-0.001	0.004	-0.001	0.000	0.000	-0.001	0.002
0.82	-0.250	7.45	34.57	93.9	0.001	1.641	18.19	60.4
	-0.1020	0.787	1.617	2.475	0.002	0.321	1.230	2.075
1.0393	0.407	0.1055	0.0468	0.0264	2.028	0.1955	0.0676	0.0344
0.4353	0.944	-0.356	0.106	-0.033	0.752	-0.284	0.067	-0.018
0.0724	0.328	0.850	-0.441	0.183	0.646	0.894	-0.395	0.145
-0.0035	-0.012	0.385	0.731	-0.511	0.127	0.344	0.793	-0.486
-0.0038	-0.026	-0.006	0.505	0.570	-0.032	-0.022	0.457	0.653
-0.0001	0.001	-0.043	0.049	0.597	-0.018	-0.038	0.020	0.553
0.0004	0.006	-0.007	-0.050	0.141	0.002	-0.005	-0.045	0.093
0.0002	0.004	0.005	-0.015	-0.048	0.002	0.005	-0.014	-0.048
0.0000	0.003	0.001	0.005	-0.030	0.002	0.001	0.006	-0.021
-0.0002	0.002	-0.001	0.005	-0.001	0.000	0.000	0.001	0.002

Table I (continued)

0.80	-0.240	6.61	31.26	85.5	0.001	1.400	16.30	54.9
	-0.0971	0.697	1.450	2.232	0.003	0.278	1.099	1.871
1.0512	0.405	0.1055	0.0464	0.0261	2.044	0.1985	0.0674	0.0341
0.4954	0.929	-0.394	0.131	-0.045	0.669	-0.313	0.083	-0.025
0.0944	0.367	0.807	-0.475	0.221	0.721	0.866	-0.429	0.177
-0.0044	-0.012	0.435	0.662	-0.530	0.173	0.386	0.739	-0.514
-0.0063	-0.038	0.000	0.555	0.468	-0.043	-0.022	0.507	0.565
-0.0004	-0.001	-0.061	0.072	0.640	-0.029	-0.054	0.037	0.603
0.0007	0.007	-0.012	-0.068	0.185	0.001	-0.006	-0.064	0.128
0.0003	0.004	0.008	-0.027	-0.058	0.004	0.007	-0.021	-0.059
0.0000	0.003	0.002	0.006	-0.045	0.002	0.002	0.008	-0.034
-0.0002	0.002	-0.002	0.008	-0.003	0.001	0.000	0.003	0.002
0.78	-0.221	5.79	28.09	77.1	0.001	1.178	14.48	49.6
	-0.0875	0.603	1.279	1.970	0.002	0.236	0.962	1.659
1.0661	0.396	0.1042	0.0456	0.0256	1.984	0.2002	0.0665	0.0334
0.5615	0.912	-0.431	0.161	-0.061	0.565	-0.342	0.101	-0.033
0.1222	0.407	0.755	-0.503	0.261	0.788	0.831	-0.461	0.211
-0.0054	-0.012	0.487	0.580	-0.536	0.234	0.433	0.675	-0.533
-0.0101	-0.054	0.011	0.604	0.352	-0.053	-0.020	0.557	0.467
-0.0009	-0.003	-0.083	0.104	0.670	-0.048	-0.074	0.058	0.643
0.0012	0.011	-0.020	-0.084	0.244	-0.001	-0.011	-0.084	0.176
0.0005	0.006	0.012	-0.042	-0.063	0.008	0.011	-0.032	-0.073
0.0000	0.002	0.005	0.008	-0.066	0.003	0.004	0.010	-0.054
-0.0002	0.002	-0.001	0.012	-0.007	0.000	0.000	0.007	0.000
0.76	-0.196	4.99	24.86	68.9	0.001	0.973	12.74	44.5
	-0.0739	0.506	1.092	1.707	0.003	0.195	0.822	1.435
1.0852	0.378	0.1014	0.0439	0.0248	1.853	0.2000	0.0645	0.0323
0.6361	0.890	-0.469	0.195	-0.081	0.446	-0.370	0.121	-0.044
0.1580	0.449	0.690	-0.523	0.300	0.836	0.787	-0.488	0.248
-0.0061	-0.009	0.538	0.486	-0.523	0.305	0.483	0.597	-0.540
-0.0159	-0.073	0.029	0.645	0.223	-0.057	-0.010	0.607	0.355
-0.0020	-0.009	-0.109	0.146	0.684	-0.072	-0.097	0.086	0.672
0.0020	0.016	-0.032	-0.106	0.317	-0.006	-0.021	-0.108	0.233
0.0010	0.009	0.018	-0.064	-0.058	0.013	0.017	-0.051	-0.084
0.0000	0.002	0.010	0.009	-0.094	0.005	0.007	0.013	-0.076
-0.0003	0.001	-0.001	0.019	-0.020	0.000	0.000	0.011	-0.004
0.74	-0.164	4.19	21.67	60.5	0.002	0.785	10.99	39.4
	-0.0573	0.404	0.899	1.410	0.003	0.154	0.675	1.207
1.1108	0.349	0.0963	0.0415	0.0233	1.639	0.1959	0.0614	0.0306
0.7230	0.862	-0.507	0.233	-0.107	0.312	-0.396	0.144	-0.058
0.2054	0.496	0.609	-0.530	0.340	0.859	0.734	-0.509	0.288
-0.0061	0.001	0.587	0.372	-0.490	0.386	0.533	0.505	-0.531
-0.0252	-0.098	0.058	0.676	0.083	-0.059	0.001	0.651	0.225
-0.0041	-0.020	-0.141	0.208	0.669	-0.107	-0.130	0.131	0.686
0.0036	0.022	-0.055	-0.123	0.397	-0.014	-0.036	-0.131	0.305
0.0019	0.014	0.025	-0.102	-0.045	0.023	0.024	-0.077	-0.076
-0.0001	0.001	0.020	0.005	-0.133	0.011	0.014	0.015	-0.109
-0.0004	0.000	0.001	0.030	-0.037	-0.002	-0.001	0.021	-0.015

Table I (continued)

0.72	-0.129	3.38	18.63	52.4	0.003	0.600	9.23	34.0
	-0.0392	0.296	0.700	1.124	0.004	0.112	0.518	0.955
1.1465	0.305	0.0876	0.0376	0.0214	1.323	0.1866	0.0561	0.0281
0.8289	0.830	-0.543	0.277	-0.140	0.159	-0.421	0.170	-0.076
0.2714	0.541	0.503	-0.519	0.372	0.847	0.668	-0.519	0.326
-0.0043	0.016	0.632	0.239	-0.419	0.478	0.585	0.391	-0.494
-0.0404	-0.126	0.100	0.690	-0.070	-0.049	0.020	0.686	0.076
-0.0087	-0.037	-0.180	0.280	0.617	-0.155	-0.172	0.191	0.671
0.0066	0.030	-0.089	-0.136	0.496	-0.031	-0.057	-0.161	0.399
0.0040	0.024	0.032	-0.148	0.005	0.038	0.037	-0.119	-0.062
-0.0003	0.001	0.036	0.000	-0.171	0.020	0.026	0.018	-0.153
-0.0010	-0.003	0.003	0.045	-0.069	-0.003	-0.002	0.037	-0.037
0.70	-0.099	2.58	15.54	44.4	0.006	0.447	7.67	28.7
	-0.0238	0.191	0.499	0.818	0.006	0.075	0.370	0.714
1.1996	0.240	0.0740	0.0321	0.0184	1.005	0.1689	0.0482	0.0248
0.9648	0.790	-0.575	0.326	-0.187	0.017	-0.439	0.201	-0.099
0.3675	0.583	0.368	-0.476	0.392	0.789	0.585	-0.521	0.365
0.0010	0.034	0.660	0.084	-0.307	0.569	0.635	0.256	-0.433
-0.0663	-0.165	0.159	0.670	-0.224	-0.017	0.060	0.699	-0.070
-0.0185	-0.060	-0.218	0.382	0.501	-0.209	-0.214	0.264	0.610
0.0122	0.046	-0.144	-0.126	0.591	-0.066	-0.097	-0.176	0.498
0.0090	0.041	0.035	-0.212	0.091	0.053	0.046	-0.173	-0.006
-0.0006	-0.001	0.063	-0.020	-0.210	0.038	0.046	0.016	-0.196
-0.0024	-0.009	0.011	0.066	-0.121	-0.002	0.002	0.059	-0.078

is indicated immediately before the first subtable. The first column lists respectively the value of x to which the subtable applies, the volume-preserving normalization constant $\hat{\lambda} = \lambda(\hat{\underset{\sim}{\alpha}})$, and the 9 even $\hat{\alpha}_n$ which define the saddle point. [The values of $\hat{\alpha}_n$ used here were calculated with the same computer code that was used in Ref. (8) but with a higher specified accuracy; they are therefore in some cases slightly different from the corresponding values tabulated in Ref. (8).] Columns 2 through 5 list the properties of the 4 lowest symmetric normal modes (n = 2, 4, 6 and 8) and columns 6 through 9 the 4 lowest asymmetric modes (n = 1, 3, 5 and 7). The first entry in each of the last 8 columns gives the square of the frequency in natural units of $E_s^{(0)}/(M_0R_0^2)$; the second and third entries in each column give respectively the normal-coordinate stiffness constant in units of $E_s^{(0)}$ and inertia constant in units of $M_0R_0^2$. The final 9 entries of each column give the elements of the eigenvector that are not zero from symmetry considerations.

As will be discussed later the stiffness constant K_1 measures the restoring force against displacements of the drop's center of mass, and in a calculation with infinite accuracy both it and the corresponding frequency ω_1 would of course be identically zero. The small departures from zero of the calculated values of K_1 and ω_1 listed in Table I provide some estimate of the accuracy of the present calculations. For many of the entries in Table I the last figure reported is uncertain by a few units, and in a few cases where 4 figures are given the last 2 figures are uncertain.

The squares of the 6 lowest frequencies in natural liquid-drop units are shown as functions of x in Fig. 1. (Short-dashed lines are used in this and in the following figures to indicate results that are of questionable accuracy.) The magnitudes of the 6 lowest frequencies in MeV are shown in Fig. 2 for nuclei along Green's approximation to the line of beta stability (21). In converting from liquid-drop units to MeV the values of Myers and Swiatecki have been used for the constants of the semiempirical mass formula (6).

The new mass formula of Myers and Swiatecki attempts to isolate that portion of the mass associated exclusively with nuclear shell structure from the purely liquid-drop portion of the mass and as such is believed to represent a fairly accurate determination of the constants of the semi-

empirical mass formula. This mass formula takes into account also the dependence of the surface energy on nuclear composition (i.e. the difference N-Z between neutron and proton numbers) and the dependence of the Coulomb energy on the diffuseness of the charge distribution. As a result of the inclusion of a composition dependence in the surface energy, the fissility parameter x is no longer proportional simply to Z^2/A but depends also explicitly upon N-Z. When the Myers-Swiatecki constants are used the fissility parameter is given by

$$x = \frac{(Z^2/A)}{51.77\left[1 - 1.79\left(\frac{N-Z}{A}\right)^2\right]} \quad . \tag{20}$$

Similarly the unit of frequency multiplied by $\hbar$ is

$$\hbar\left[E_s^{(0)}/(M_0R_0^{\,2})\right]^{\frac{1}{2}} = \frac{23.12\left[1 - 1.79\left(\frac{N-Z}{A}\right)^2\right]^{\frac{1}{2}}}{A^{\frac{1}{2}}}\ \text{MeV} \quad . \tag{21}$$

Since the even-numbered modes consist of a linear combination of the even Legendre polynomials, they correspond to deviations from the saddle point that preserve inversion symmetry and reflection symmetry at a plane through the origin perpendicular to the symmetry axis; conversely the odd-numbered modes destroy these symmetries. Each of the lower modes has a direct physical interpretation, which we will now discuss in turn.

The lowest asymmetric mode (n = 1) is a pure center-of-mass shift of the drop; its restoring force against displacements and its frequency are consequently zero for all values of x.

The lowest symmetric mode (n = 2) is an <u>unstable</u> motion in the "fission" direction, leading either to the division of the drop or to the return of the drop to a pre-saddle-point configuration. Since for this mode the square of the frequency is negative (zero for x = 1) the frequency itself is purely imaginary. The magnitude of ω_2 (which we denote by $|\omega_2|$) determines to a large extent the probability that a nucleus with a given amount of energy concentrated in the fission direction will penetrate the fission barrier. Small values of $|\omega_2|$ correspond to relatively flat barriers with small penetrabilities whereas large values correspond to relatively thin barriers with large penetrabilities. From Fig. 2 we see that

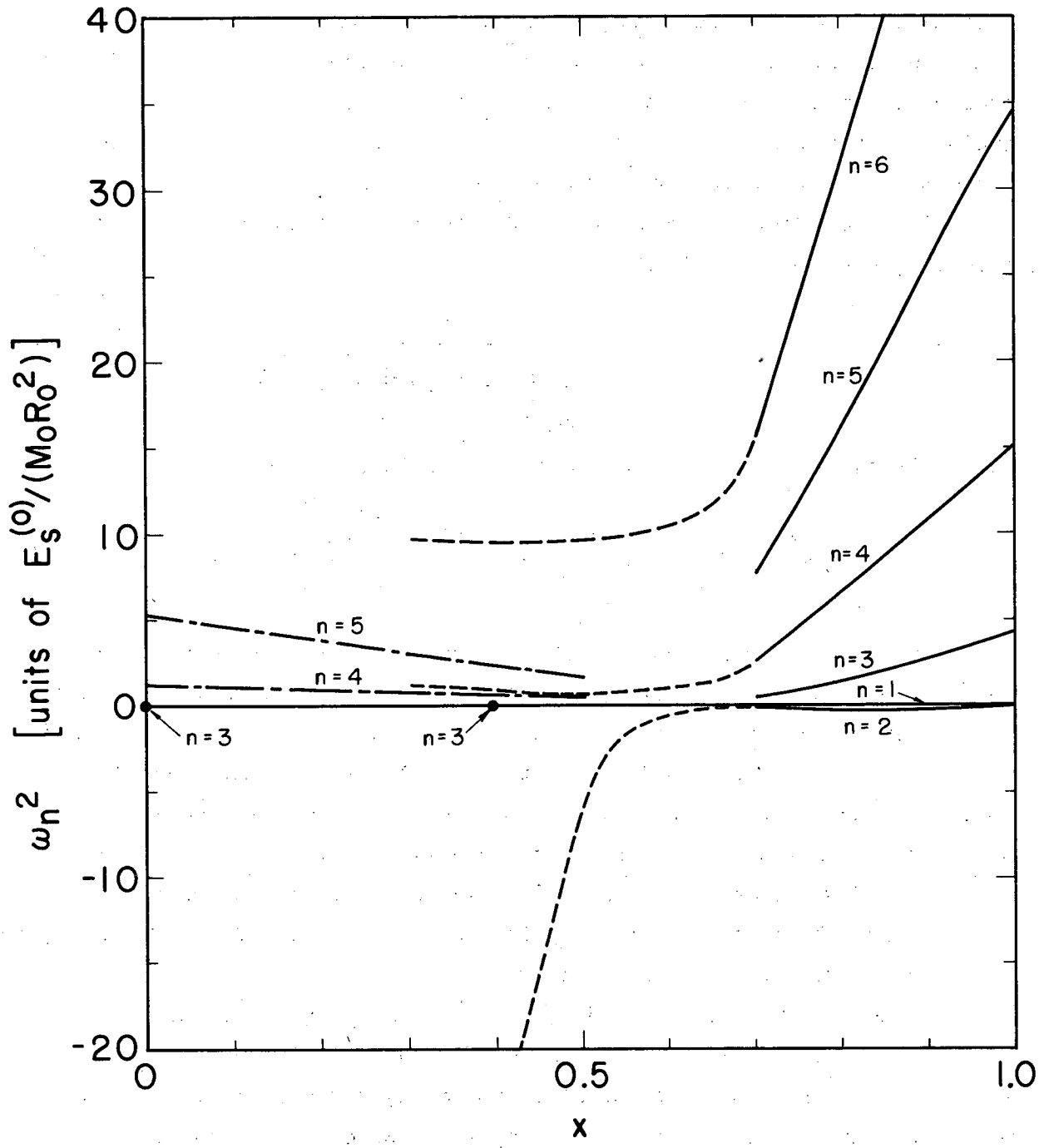

Fig. 1. Squares of the 6 lowest frequencies in natural liquid-drop units of $E_s^{(0)}/(M_0R_0^2)$ as functions of the fissility parameter x. The portions of the curves indicated by the short-dashed lines are of questionable accuracy. The solid points give the locations of the known zeros (at $x = x_{BG} = 0.39_4$ and at $x = 0$) of the $n = 3$ curve. In addition the results obtained for $n = 4$ and $n = 5$ in the two-spheroid approximation (3) are shown for $x \leq 0.5$ by the dot-dashed lines.

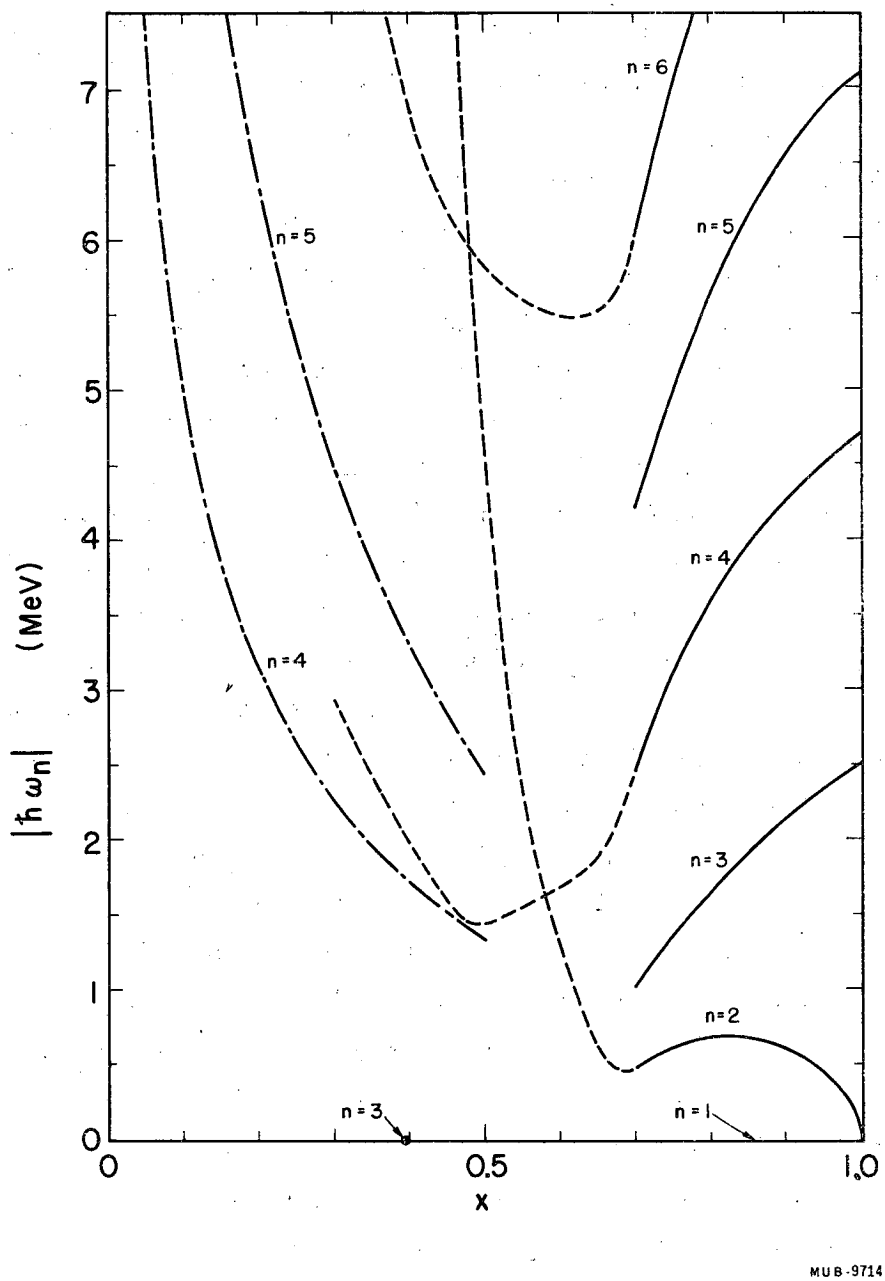

Fig. 2. Magnitudes of the 6 lowest frequencies in MeV for nuclei along Green's approximation (21) to the line of beta stability as functions of the fissility parameter x. The values used for the constants of the semiempirical mass formula are those of Myers and Swiatecki (6). The portions of the curves indicated by the short-dashed lines are of questionable accuracy. The solid point gives the location of the known zero (at $x = x_{BG} = 0.39_4$) of the n = 3 curve. In addition the results obtained for n = 4 and n = 5 in the two-spheroid approximation (3) are shown for $x \leq 0.5$ by the dot-dashed lines.

as a function of decreasing x the magnitude of $\hbar\omega_2$ initially increases from 0 at x = 0 to a local maximum of about 0.7 MeV at $x \approx 0.82$ and then decreases to a local minimum of about 0.45 MeV at $x \approx 0.68$. This is followed by a very rapid increase in $|\hbar\omega_2|$ as x is decreased further; for example at x = 0.5 it is already almost 5 MeV. This implies that the fission barrier for a very light nucleus should be exceedingly penetrable and consequently that the fission cross section for such a nucleus should vary relatively slowly with excitation energy in the neighborhood of the fission barrier. Furthermore because of the large probability of fissioning at excitation energies below the top of the barrier, experimentally determined barrier heights for the lighter nuclei would be expected to be incorrect unless proper account were taken of barrier penetration.

The lowest nonzero asymmetric mode (n = 3) is a mass-asymmetric oscillation of the drop. It is seen from Fig. 2 that the frequency of this mode decreases from about 2.5 MeV at x = 0 to about 1 MeV at x = 0.7. In addition we know from Ref. (8) that ω_3^2 remains positive as long as x is greater than $x_{BG} = 0.39_4$, but that ω_3^2 becomes negative and the mass-asymmetric mode is consequently unstable for $x < x_{BG}$. This known value of x at which ω_3^2 changes sign is shown by a solid point in each of Figs. 1, 2 and 3. The second known zero of ω_3^2 at x = 0 is also indicated by a solid point in Fig. 1. This result follows because at x = 0 the saddle-point shape consists of two touching spheres and therefore has zero neck radius. Since the inertia constant for a flow of mass through a neck or an aperture of zero radius is infinite (3,22) the corresponding n = 3 mass-asymmetric frequency is zero.

For smaller values of x the frequencies for n = 4 and n = 5 have been previously estimated on the basis of a two-spheroid parametrization of fission shapes (3), and for $x \leq 0.5$ these estimates are also included in Figs. 1 and 2. For small values of x the n = 4 mode, which is the lowest stable symmetric mode, corresponds to an in-phase stretching and contraction of the two halves of the saddle-point configuration. Similarly the n = 5 distortion-asymmetric mode corresponds to an out-of-phase stretching and contraction.

We note in Fig. 1 that apart from ω_1^2 and ω_2^2 the general behavior of the frequencies when plotted in natural liquid-drop units is to decrease

initially with decreasing x and then to remain fairly independent of x. On the other hand, we see in Fig. 2 that when plotted in MeV the frequencies increase rapidly for very low values of x. This follows from dimensional analysis: note the $A^{\frac{1}{2}}$ in the denominator of Eq. (21) for the magnitude in MeV of the natural liquid-drop unit of frequency.

We present in Fig. 3 the dependences on fissility parameter of the stiffness constants for the 6 lowest modes, and in Fig. 4 those of the corresponding inertia constants. Recall that both the stiffness and inertia constants depend explicitly upon how the eigenvectors are normalized [Eq. (17)]. As an illustration of this statement note in Fig. 4 that with our choice of normalization the inertia constant M_1 corresponding to center-of-mass shifts does not remain constant at 1 but instead varies with x. On the other hand, it is often worthwhile to examine the relative values of the stiffness and inertia constants. For example at low values of x the inertia constant M_2 for motion in the fission direction is seen to be much smaller than the other normal-coordinate inertia constants. Physically this is because at low values of x the fission mode consists primarily of a contraction or pinching in of the drop's neck and consequently displaces very little mass. This is to be contrasted with the erroneous but often-made assumption that the fission mode is for all values of x a separation of the centers of mass of the two halves of the drop. As x approaches 0 the amount of mass displaced in the fission mode approaches 0 and consequently ω_2^2 approaches $-\infty$ (see again the n = 2 curve in Fig. 1).

Information regarding the eigenvectors is presented in Figs. 5a and 5b. Shown are the distortions from the saddle point associated with the 6 lowest normal modes for x = 0.9, 0.8 and 0.7. In each case the saddle-point shape is indicated by a dashed line; the shapes obtained by displacing the appropriate normal coordinate by +0.2 and by -0.2 are indicated respectively by dark and by light solid lines.

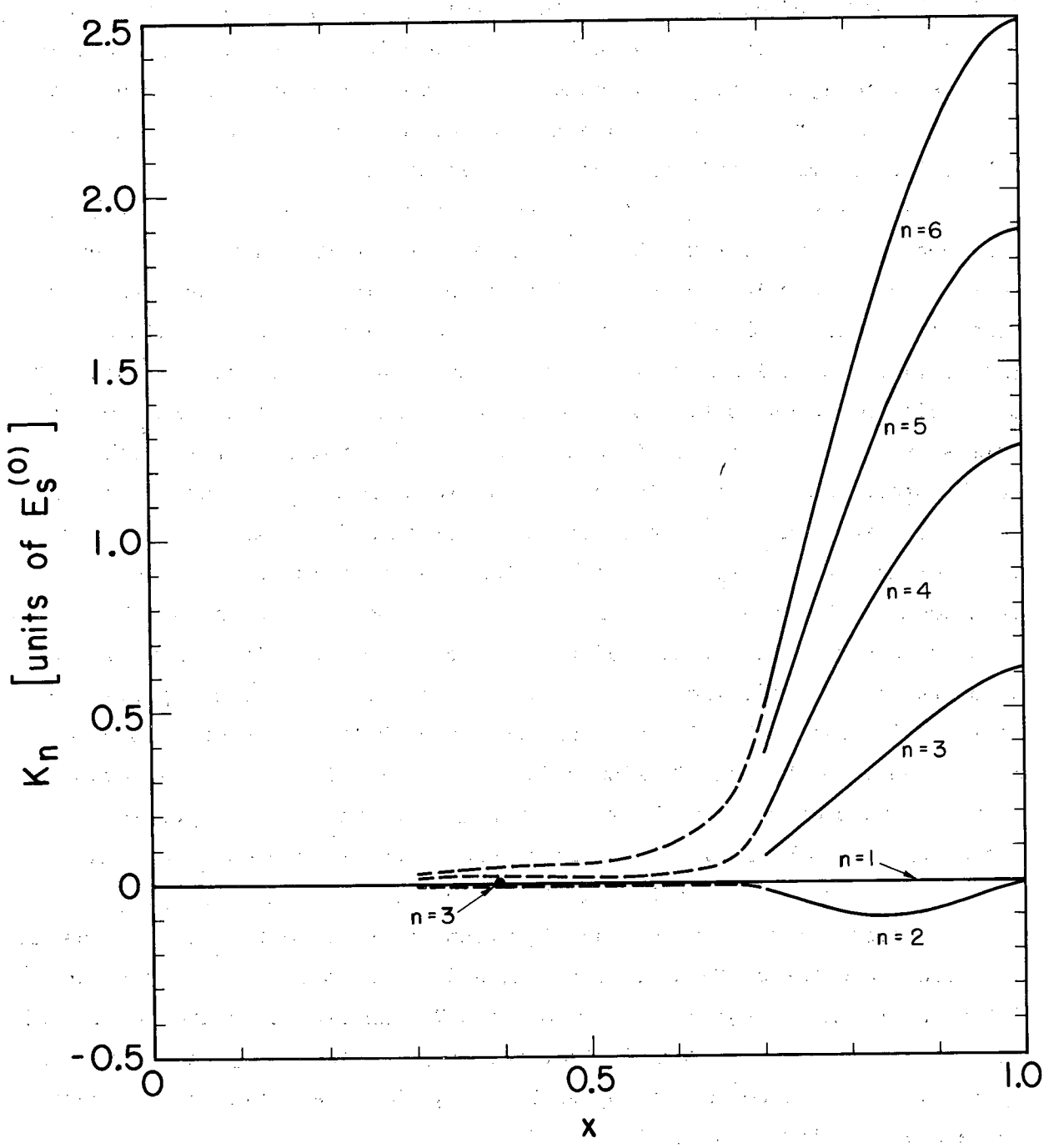

MUB-9715

Fig. 3. The normal-coordinate stiffness constants for the 6 lowest modes as functions of the fissility parameter x. The portions of the curves indicated by the dashed lines are of questionable accuracy. The location of the known zero (at $x = x_{BG} = 0.39_4$) of the n = 3 curve is shown by the solid point.

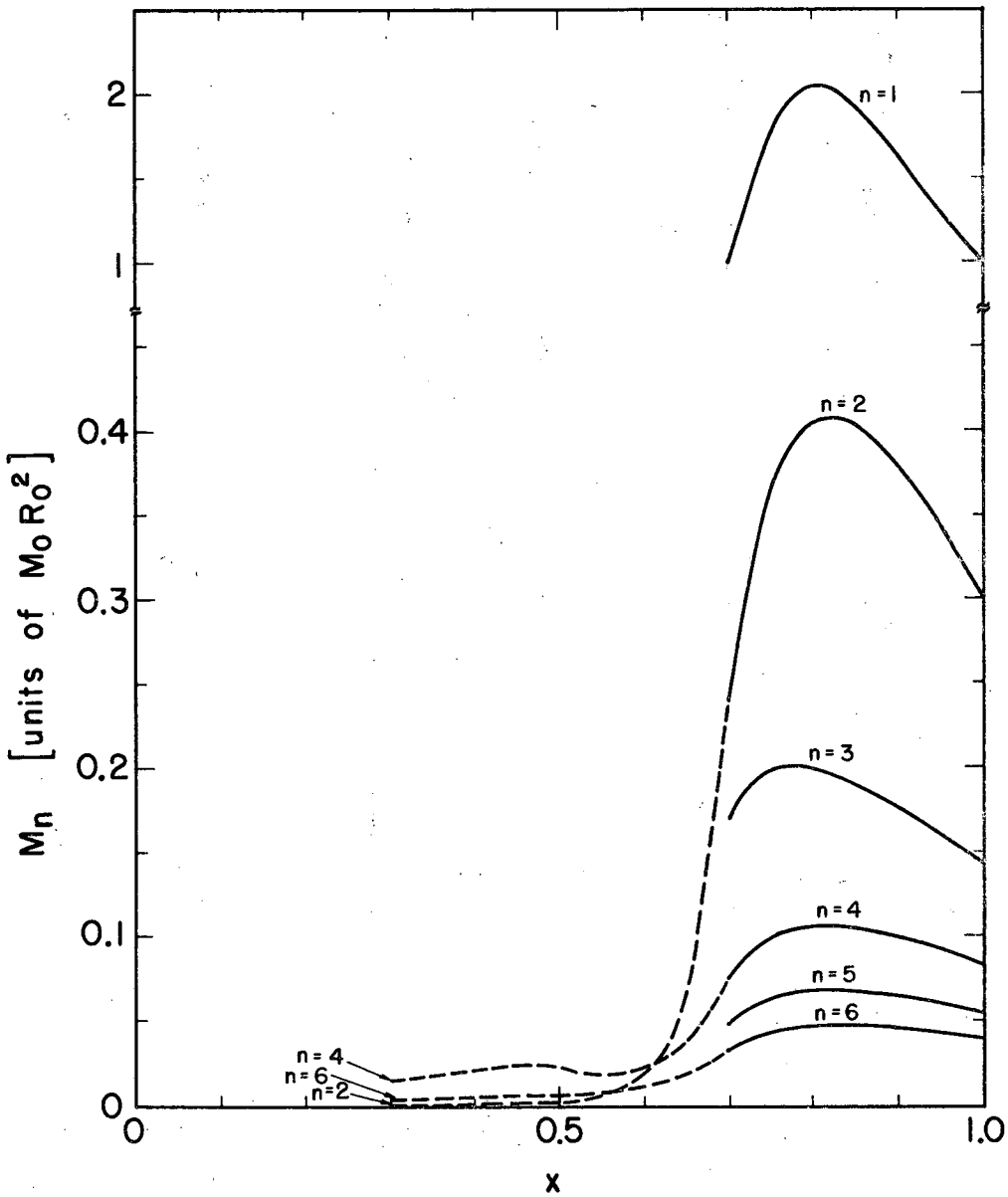

MUB-9716

Fig. 4. The normal-coordinate inertia constants for the 6 lowest modes as functions of the fissility parameter x. The portions of the curves indicated by the dashed lines are of questionable accuracy. Note that the scale is discontinuous: the n = 1 curve is plotted on a scale reduced by 10.

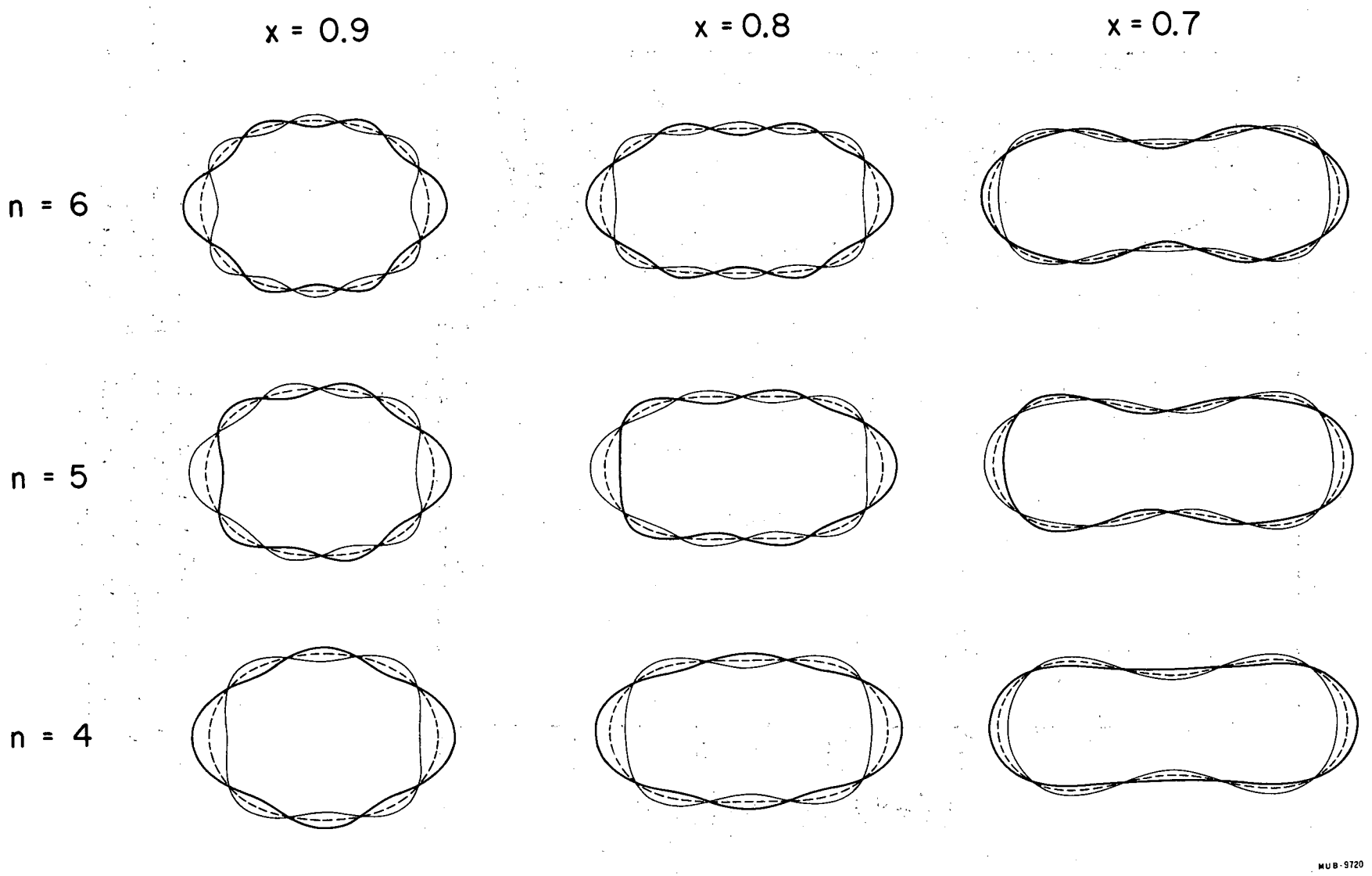

Fig. 5a. Distortions associated with the n = 6, 5 and 4 normal modes for x = 0.9, 0.8 and 0.7.

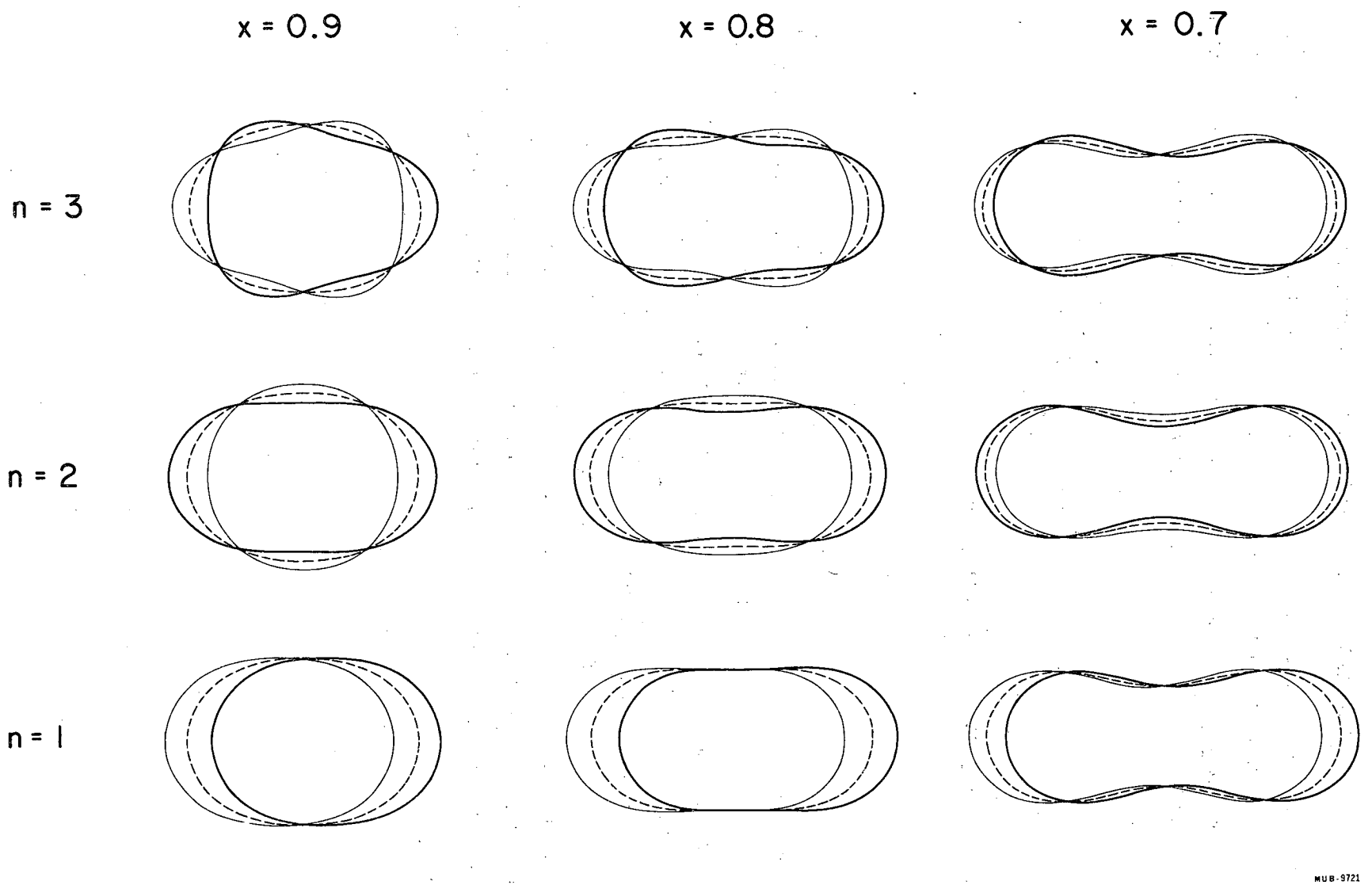

Fig. 5b. Distortions associated with the n = 3, 2 and 1 normal modes for x = 0.9, 0.8 and 0.7.

IV. APPLICATIONS AND COMPARISON WITH EXPERIMENTAL DATA

The present calculations are directly applicable to the discussion of the motion of an idealized fissioning nucleus near its saddle point. In terms of the normal coordinates and their conjugate momenta the Hamiltonian near the saddle point is simply a sum of harmonic-oscillator Hamiltonians, i.e.

$$\mathcal{H} - \hat{\mathcal{H}} = \mathcal{V} - \hat{\mathcal{V}} + \mathcal{T} = \frac{1}{2} \sum_{n=1}^{N} \left(K_n \beta_n^{\,2} + \frac{p_n^{\,2}}{M_n} \right) \quad ,$$

where the conjugate momenta are given by

$$p_n = M_n \dot{\beta}_n \quad .$$

The stiffness constants K_n, inertia constants M_n and normal coordinates β_n for the 8 lowest normal modes have been tabulated in the preceding section.

The motion of the system near the saddle point consists of a superposition of the motions of the independent harmonic oscillators. We have seen that the two—and in some cases three—lowest oscillators have zero or negative stiffness constants and therefore correspond to unbounded motions: The n = 1 mode is a shift of the drop's center of mass, and the n = 2 mode represents unstable motion in the fission direction. For $x < x_{BG} = 0.39_4$ the n = 3 mass-asymmetric mode is also unstable. The remaining oscillators have positive stiffness constants and therefore correspond to bounded motions.

A. Transition-State Energy Levels of Collective Oscillations

The frequencies of the stable oscillators are relevant as regards the spectrum of quantum states of a nucleus in the vicinity of its saddle point (23), i.e. at its transition state. Reference (24) contains an early discussion of the concept of a transition state, where it is employed in connection with the rates of molecular reactions. In general the transition-state method consists of dividing a system of N degrees of freedom into 2 systems at its saddle point: a system having a single degree of freedom that represents unstable motion (proceeding toward molecular reaction, fission etc., depending upon the physical situation) and a second system associated with the remaining N-1 degrees of freedom. (The second system can be obtained by assigning in the original system a fixed value to the normal coordinate representing unstable motion, e.g. in our case by setting β_2 equal to 0.) The total wave function for the original system is the product of the wave function for the first system in 1 degree of freedom and the wave function for the second system in the remaining N-1 degrees of freedom. It is therefore of interest to discuss the various properties of the reduced system of N-1 degrees of freedom. Its quantum energy levels are of particular interest; for the reduced system they represent stationary states, but of course are decaying states of the original system.

The transition-state spectrum of a nucleus of course contains many levels with which we are not concerned—single-particle excitations, non-axially symmetric collective vibrations and rotational states. For the discussion of these levels a model with more degrees of freedom than are considered here would be required. However, axially symmetric collective vibrations at the transition state could be discussed in terms of the present calculations. For example from Fig. 2 we see that for a typical heavy nucleus the energy of the n = 3 mass-asymmetric oscillations would be expected to be slightly greater than 1 MeV. As more experimental information about transition-state spectra becomes available it should be possible to identify among the low-lying levels of various nuclei their mass-asymmetric modes and associated rotational bands, and to compare the experimental values of $\hbar\omega_3$ with the predictions of the liquid-drop model.

Various aspects of transition-state spectra, including their experimental determination through measurements of fragment angular distributions, have recently been discussed in Refs. (5) and (25). In Ref. (5) some estimates of the liquid-drop mass-asymmetric and bending frequencies are also made on the basis of prescribed deviations from approximate spheroidal saddle-point shapes; their estimates for ω_3 are somewhat larger than the results of our calculations.

B. Probability Distributions for the Saddle-Point States of Motion

In addition to the energies of its quantum states, it is desirable to know at the moment a nucleus passes through the vicinity of its saddle point (i.e. at the moment when the fission coordinate β_2 is zero) the probabilities that the bounded normal coordinates are displaced from their equilibrium values by given amounts and that their conjugate momenta have specified values.

By making the standard assumption of the transition-state method (24,26)—that statistical equilibrium is established by the time the system arrives in the vicinity of the saddle point—one can derive extremely simple expressions for the quantal probabilities that the normal coordinates and their conjugate momenta have given values. The resulting expressions are Gaussian distributions in the coordinates and momenta (3,27,28):

$$P(\beta_n) = (\pi C_n)^{-\frac{1}{2}} \exp(-\beta_n{}^2/C_n)$$

and

$$P(p_n) = (\pi C_n{}')^{-\frac{1}{2}} \exp(-p_n{}^2/C_n{}') \quad ,$$

where the temperature-dependent constants C_n and $C_n{}'$ are given explicitly by

$$C_n = \frac{\hbar\omega_n}{K_n} \coth\left(\frac{\hbar\omega_n}{2\Theta}\right) \rightarrow \begin{cases} 2\Theta/K_n & , \quad \Theta \gg \hbar\omega_n \\ \hbar\omega_n/K_n & , \quad \Theta \ll \hbar\omega_n \end{cases}$$

and

$$C_n{}' = M_n \hbar\omega_n \coth\left(\frac{\hbar\omega_n}{2\Theta}\right) \rightarrow \begin{cases} 2M_n\Theta & , \quad \Theta \gg \hbar\omega_n \\ M_n\hbar\omega_n & , \quad \Theta \ll \hbar\omega_n \end{cases} \quad .$$

The nuclear temperature Θ is a function of the internal nuclear excitation energy at the saddle point. Note that for high temperatures the above quantal expressions reduce to the classical results, whereas in the low-temperature limit they reduce to the distributions for the quantal zero-point motions of harmonic oscillators.

By tracing out dynamically a drop's division and the separation of its fragments to infinity one could convert the above probability distributions for the initial states of motion near the saddle point into probability distributions for the final states of motion of the fragments at infinity. These correspond to such observable fission-fragment properties as their division of mass, their translational kinetic energies and their excitation energies. Since the stiffness and inertia constants and the frequencies have been calculated in the previous sections, probability distributions for the initial states of motion are completely known. This would make it possible to compare directly the measured and predicted probability distributions without the use of any adjustable parameters, provided only that the appropriate dynamical calculations connecting the initial and final states of motion were performed. Such an approach has been carried through with moderate success for the fission of nuclei lighter than about radium, where saddle-point shapes are sufficiently dumbbell-like to permit the neglect of the dynamical descent from the saddle point to scission (3), but for heavier elements the appropriate dynamical calculations remain an open question.

C. Penetration of the Fission Barrier

Whereas for the bounded oscillations the calculated frequencies are relevant as regards the transition-state spectrum and the probability distributions for the initial states of motion, for the unstable fission mode the (purely imaginary) frequency ω_2 determines the degree of penetration of the barrier against fission. Because of its connection with barrier penetration, ω_2 can be determined experimentally from measurements of fission probabilities. Several different types of such measurements can in fact be used, e.g. fission widths, spontaneous-fission lifetimes and the variation of fission cross sections with excitation energy.

The basic formula for the fission width Γ_f follows directly from the transition-state theory of reaction rates (11,29):

$$\Gamma_f(E^*) = \frac{N_f(E^*)}{2\pi\rho(E^*)} \quad , \tag{22}$$

where $\rho(E^*)$ is the density of levels in the compound nucleus at an excitation energy E^* (relative to the ground-state energy, which includes the sum of all relevant zero-point energies of the ground-state configuration) and $N_f(E^*)$ is the effective number of open channels at the saddle-point configuration. (It is understood in this discussion that the levels are to have the appropriate quantum numbers.) The effective number of channels $N_f(E^*)$ is the sum over the individual levels in the transition-state spectrum of the probabilities for penetrating the fission barrier when the specific levels are excited, i.e.

$$N_f(E^*) = \sum_i P_i(E^*, X_i) \quad , \tag{23}$$

where X_i is the energy of the ith quantum state at the saddle point for the nonfission degrees of freedom (relative to the energy of the lowest state, which includes the sum of the relevant zero-point energies at the saddle point).

The exact determination of the penetrability $P_i(E^*, X_i)$ would in general involve the solution of a nonseparable Schrödinger equation in many dimensions. However, if the coordinate for motion in the fission direction

were not coupled with the remaining coordinates (i.e. if the Hamiltonian could be written as the sum of a term that depends only upon the fission coordinate and a second term that depends only upon the nonfission coordinates) the problem would separate into a one-dimensional barrier-penetration problem in the fission degree of freedom and into a second problem involving the remaining (nonfission) degrees of freedom. The solution of the first problem would determine the penetrability, and the solution of the second the energies X_i of the quantum states, which would be identical at the saddle point and at the ground state by virtue of their (assumed) independence of the fission coordinate. In particular the sum of the zero-point energies associated with the nonfission degrees of freedom would not change from the ground state to the saddle point. The diagram in Fig. 6 illustrates these and other energies that we shall discuss.

In order for the fission coordinate to be regarded as uncoupled for the purpose of calculating penetrabilities, it is necessary that it be effectively uncoupled in the region from the ground state to the position where the system emerges after having passed through the fission barrier. When x is close to 1 this is in fact approximately the case. However, for arbitrary values of x the fission degree of freedom is <u>not</u> uncoupled from the rest: we have seen for example that the frequencies and eigenvectors of the normal modes at the saddle point are in general significantly different from those at the ground state.

Inherent in all existing discussions of fission-barrier penetration is the implied assumption that the fission degree of freedom is uncoupled from the other degrees of freedom. With the above reservations in mind we will also make this assumption here. It should be stressed, however, that the relationship between the solution of the resulting one-dimensional problem and an exact solution of the original multidimensional problem is unknown and represents an important question that should be thoroughly investigated.

For a given one-dimensional potential-energy fission barrier and also a given dependence of the effective mass on deformation, the penetrability $P_i(E^*,X_i)$ is determined by solving Schrödinger's equation in one dimension. For certain simple barrier shapes and effective masses, closed forms for the penetrability can be obtained either exactly or by use of the WKB approximation. For example if it is assumed that the fission barrier is everywhere

Fig. 6. An illustration of the relevant energies for a system in which the fission coordinate is uncoupled from the nonfission coordinates. The open circle denotes the ground-state energy, which is made up of the sum of all the relevant zero-point energies of the ground-state configuration, i.e. $\frac{1}{2}\hbar\omega_{gs}$ for the fission degree of freedom and the sum Σ_{nf} of the zero-point energies for the nonfission degrees of freedom. The ground-state energy serves as the reference line from which the total excitation energy E^* brought into the nucleus is measured. However, the total energy relative to the minimum of the potential-energy curve is obtained by adding to E^* the zero-point energy $\frac{1}{2}\hbar\omega_{gs}$ in the fission degree of freedom. To obtain the total energy E in the fission degree of freedom, which is the quantity relevant for barrier penetration, one must subtract from the sum $E^* + \frac{1}{2}\hbar\omega_{gs}$ the excitation energy X in the nonfission degrees of freedom. For a chosen point along the fission direction the energy E is shown divided into the potential energy V at that point and the kinetic energy T in the fission degree of freedom. The potential-energy fission barrier of height B is idealized here as cubic in shape. For an uncoupled system the sum Σ_{nf} of the zero-point energies for the nonfission degrees of freedom does not change during the process and consequently need not be considered.

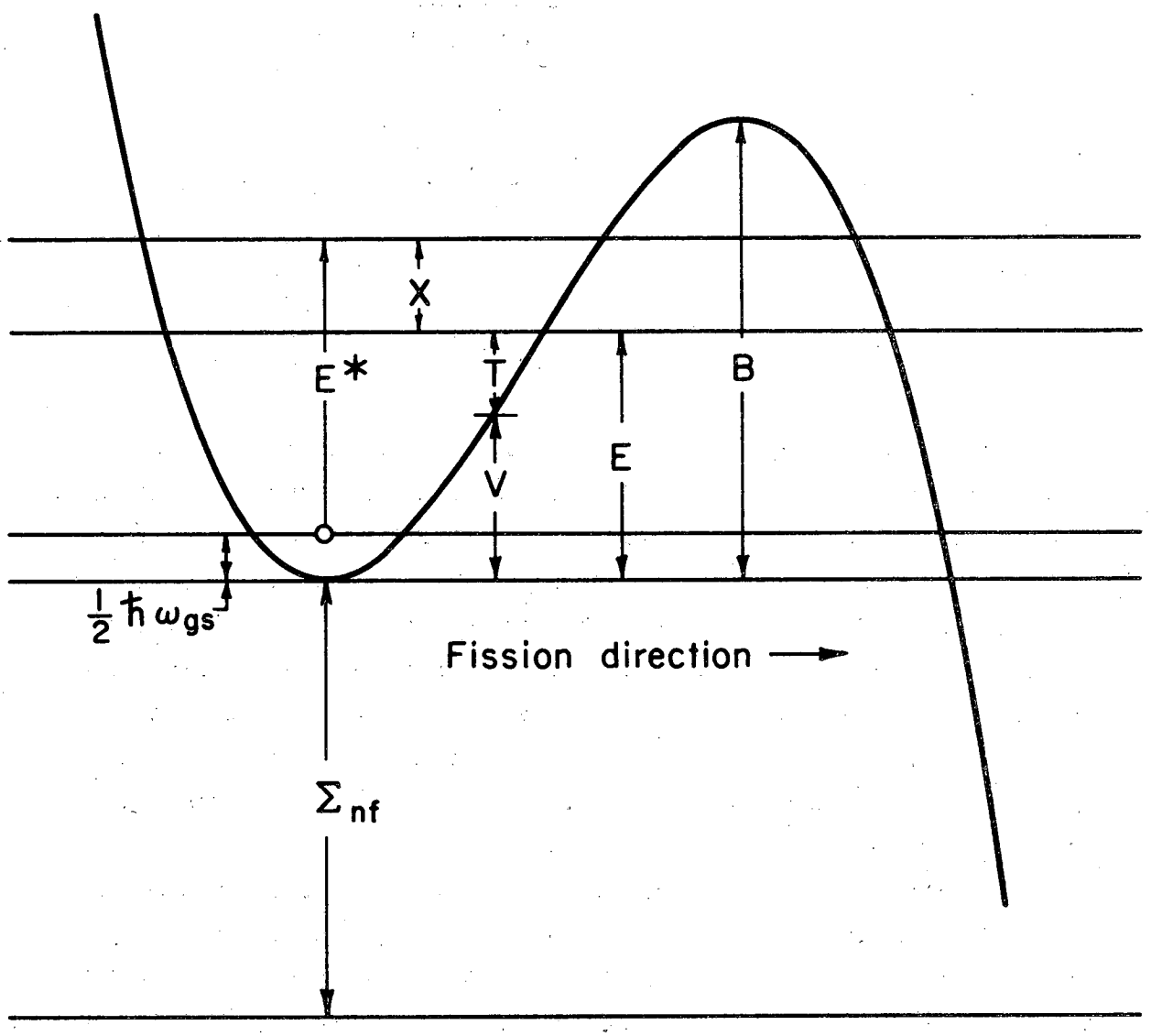

MUB-10350

Fig. 6.

parabolic and that the effective mass is constant the penetrability is given exactly by (1,29,30)

$$P_i(E^*,X_i) = \frac{1}{1 + \exp[\gamma(E)]} \quad , \tag{24a}$$

where

$$\gamma(E) = \frac{2\pi(B - E)}{\epsilon} \quad ; \tag{24b}$$

the energy ϵ is defined by

$$\epsilon = |\hbar\omega_2| \quad ,$$

and we will use this notation for the remainder of our discussion. (A variety of symbols has been used to denote this same quantity, including E_{curv}, $\hbar\omega_{imag}$, $\hbar\omega_b$, $\hbar\omega_f$ and simply $\hbar\omega$.) As can be quickly verified by consulting Fig. 6 the combination B - E represents the energy deficit in the fission degree of freedom relative to the top of the barrier and is equal to $B + X_i - \frac{1}{2}\hbar\omega_{gs} - E^*$. In many cases the true shape of the fission barrier is approximately parabolic near its maximum, and for such cases Eqs. (24) should be fairly accurate as long as E is not significantly less than B. On the other hand, when E is very small, as in spontaneous fission, Eq. (24b) would be expected to be somewhat in error.

For the important case in which the low-lying transition-state levels are widely separated and also $E^* + \frac{1}{2}\hbar\omega_{gs} \lesssim B$ the probabilities for penetration through the higher levels are negligible in comparison with the lowest level that has the appropriate quantum numbers, and the sum in (23) reduces to a single term. Thus for the case of fission through a parabolic barrier with widely separated transition-state levels Eq. (22) becomes

$$\Gamma_f(E^*) \approx \frac{1}{2\pi\rho(E^*)\left\{1 + \exp\left[\frac{2\pi(B + X_L - \frac{1}{2}\hbar\omega_{gs} - E^*)}{\epsilon}\right]\right\}} \quad , \tag{25}$$

where X_L is the energy of the lowest quantum state at the saddle point for the nonfission degrees of freedom that has the appropriate quantum numbers.

When $E^* + \frac{1}{2}\hbar\omega_{gs}$ is somewhat smaller than $B + X_L$ the exponential term is large in comparison with unity, and (25) assumes the form

$$\Gamma_f(E^*) \approx \frac{1}{2\pi\rho(E^*)} \exp\left[\frac{-2\pi(B + X_L - \frac{1}{2}\hbar\omega_{gs} - E^*)}{\epsilon}\right] . \tag{26}$$

However, when the excitation energy is very small, say zero as in spontaneous fission, Eq. (26) can be improved in two ways. First of all the transition-state method, which is based upon statistical arguments, cannot be expected to produce the exact fission width for very small excitation energies. However, when the excitation energy is 0 we know for an uncoupled system the exact WKB result (30): the spontaneous fission rate $\Gamma_f(0)/\hbar$ is equal to the product of the penetrability and the number of times per unit time $\omega_{gs}/(2\pi)$ that the barrier is assaulted. Thus the width for spontaneous fission through a parabolic barrier is approximately

$$\Gamma_f(0) \approx \frac{\hbar\omega_{gs}}{2\pi} \exp\left[\frac{-2\pi(B - \frac{1}{2}\hbar\omega_{gs})}{\epsilon}\right] . \tag{27}$$

We have set X_L equal to 0 since for spontaneous fission in an uncoupled system the lowest state at the saddle point has the appropriate quantum numbers; the total energy E in the fission degree of freedom is consequently $\frac{1}{2}\hbar\omega_{gs}$.

We note that the result (26) of the transition-state method would formally include the case of spontaneous fission provided that for zero excitation energy the average level spacing $D(0) = 1/\rho(0)$ be interpreted as the distance $\hbar\omega_{gs}$ between the levels of the fission degree of freedom rather than the average distance between the levels in all the degrees of freedom. For cases in which Eq. (26) is applicable this interpretation in fact represents a good approximation for D(0). Recall that in the derivation of Eq. (26) it was assumed that the levels are widely separated at the saddle point (and consequently for an uncoupled system also at the ground state). In these cases the ground-state energies for the nonfission degrees of freedom are comparable with or larger than $\hbar\omega_{gs}$ and do not seriously alter the average value of D(0).

If the fission coordinate were truly uncoupled from the remaining coordinates ω_{gs} would be simply the frequency of the ground-state oscilla-

tions in the fission degree of freedom. This is of course in practice not the case, and as pointed out above the true determination of the fission rate would in general involve a more detailed analysis. However, to the extent that the system can be regarded as approximately uncoupled and Eq. (27) can be regarded as approximately applicable, the frequency of the ground-state second-order spherical-harmonic (beta) vibrations can be used as a rough estimate of ω_{gs}. In the liquid-drop model the frequency of these oscillations is given exactly for all values of x by

$$\omega_{gs} = \left[\frac{8}{3}(1 - x)\right]^{\frac{1}{2}} \left[E_s^{(0)}/(M_0 R_0^{\ 2})\right]^{\frac{1}{2}} \quad . \tag{28}$$

For typical heavy nuclei of interest in fission the values of $\hbar\omega_{gs}$ obtained from this formula are slightly greater than 1 MeV.

For the benefit of those making a comparison with other sources we would like to point out that the pre-exponential factor of Eq. (27) differs from the corresponding factor of at least three other writers. The result of Ref. (11) includes an additional factor of 5 which is supposed to represent "the degree of degeneracy of the oscillation leading to instability." However, of the 5 coordinates corresponding to second-order spherical-harmonic distortions, 3 represent rotational degrees of freedom (say the 3 Euler angles) and 1 represents a non-axially symmetric (gamma) vibration. This leaves only 1 degree of freedom (a beta vibration) for motion in a direction leading toward instability, and the reason for having a factor of 5 in the formula is not clear to us. In Ref. (4) the frequency of barrier assaults is inadvertently set equal to $2\pi\omega_{gs}$ rather than $\omega_{gs}/(2\pi)$. Finally in Ref. (31) the pre-exponential factor of Eq. (26) is determined experimentally when E^* is equal to $B + X_L - \frac{1}{2}\hbar\omega_{gs}$ and is then assumed to represent also the pre-exponential factor for the case of spontaneous fission in Eq. (27). Because of the neglect of the variation of $\rho(E^*)$ with E^* their result is about 10^{-7} times as large as ours.

In addition to differences in the pre-exponential factor, Eq. (27) differs from the corresponding formula of most other writers in that it includes explicitly the zero-point energy $\frac{1}{2}\hbar\omega_{gs}$ in the fission degree of freedom. The importance of taking this energy into account has been stressed in Ref. (16). However, in fact other spontaneous-fission-rate formulae implicitly include the zero-point energy since the barrier heights

in these formulae are defined experimentally and consequently relative to the zero-point energy rather than relative to the local minimum of the potential-energy curve.

The second improvement that can be made in Eq. (26) stems from the departure of the fission barrier from a parabola at very low energies. Although the true shape of the barrier is not known, there are nevertheless two firm guidelines that one should follow when choosing a shape for it: the barrier should be parabolic near its top, and it should have a local minimum corresponding to the ground-state equilibrium configuration. The cubic shape is the simplest form which satisfies these two physical requirements, and we therefore determine the penetrability for spontaneous fission on the basis of a cubic barrier whose height is B and whose second derivative at its top is the negative quantity K_2. The effective mass M_2 is assumed to be deformation independent. It should be emphasized that there is no evidence that the true shape of the fission barrier actually is cubic (except when x is close to 1, where the leading terms in an expansion of the potential energy give rise to a cubic barrier), but for spontaneous fission the assumption that it is cubic is intrinsically more reasonable than the assumption that it is parabolic.

By use of the WKB approximation one can write the penetrability of a cubic barrier in the form of Eq. (24a), where $\gamma(E)$ is expressed in terms of elementary transcendental functions and the complete elliptic integrals of the first and second kinds. This is done in Appendix B for arbitrary values of the total energy E in the fission degree of freedom from 0 to B. From a consideration of the two limiting forms of this equation for energies near the bottom and near the top of the barrier it is possible to arrive at a simple but yet very accurate expression for $\gamma(E)$ that is valid for all values of E between 0 and B, viz.

$$\gamma(E) \approx \frac{36}{5\epsilon}\left[B - E - \left(1 - \frac{2\pi}{36/5}\right) E \ln\left(\frac{B}{E}\right)\right] \quad . \tag{29}$$

This formula reproduces correctly the exact values and first derivatives at both E = 0 and E = B; for arbitrary values of E between 0 and B the results calculated from this formula for the quantity $\gamma/\left(\frac{2\pi B}{\epsilon}\right)$ of Fig. 7 differ from exact WKB results by less than 0.002. Therefore unless extreme accuracy is

required Eq. (29) can be used rather than the more complicated exact result given in Appendix B. Graphs of $\gamma(E)$ for both a parabolic and a cubic barrier are presented in Fig. 7. We also indicate by a dashed line the result that would be obtained for a cubic barrier by neglecting the logarithmic term in Eq. (29); for values of $(E/B) \lesssim 0.3$ this is an improvement over the result for a parabolic barrier but for larger values of E/B it is poorer.

For spontaneous fission through a cubic barrier the fission width can therefore be written approximately as

$$\Gamma_f(0) \approx \frac{\hbar\omega_{gs}}{2\pi} \exp\left\{ - \frac{36}{5\epsilon}\left[B - \tfrac{1}{2}\hbar\omega_{gs} - \left(1 - \frac{2\pi}{36/5}\right) \tfrac{1}{2}\hbar\omega_{gs} \ln\left(\frac{B}{\frac{1}{2}\hbar\omega_{gs}}\right)\right]\right\} . \quad (30)$$

If an even simpler expression is desired the logarithmic term can be neglected; this produces a formula that represents an improvement over the corresponding result for a parabolic barrier [Eq. (27)] and yet differs from it only by the replacement of the 2π in the exponential by 36/5.

Since for a given nucleus the quantity ϵ characterizes the curvature of the barrier at its maximum value (and in addition the associated effective mass) it is a single number, completely independent of the excitation energy E^*. (This is of course provided that the barrier itself is not affected by a change in E^*.) The use of Eq. (30) to estimate the value of this number from a measured spontaneous-fission lifetime is perhaps more reasonable than the customary procedure of deducing ϵ from a formula based on a parabolic barrier [Eq. (27)] and then remarking that its value for spontaneous fission is expected to be smaller than its value for induced fission at energies near the top of the barrier.

To summarize, we have taken as a point of departure the standard formula for the fission width that follows from the transition-state theory of reaction rates, and have tried to develop it systematically for a system in which the fission degree of freedom is uncoupled from the remaining (nonfission) degrees of freedom. For such a system we specialized to the case of widely separated levels for the nonfission degrees of freedom and gave the results for Γ_f for two types of barriers: the usual parabolic barrier and a cubic barrier, which is the more reasonable one especially for spontaneous fission. We would like to stress again, however, that in

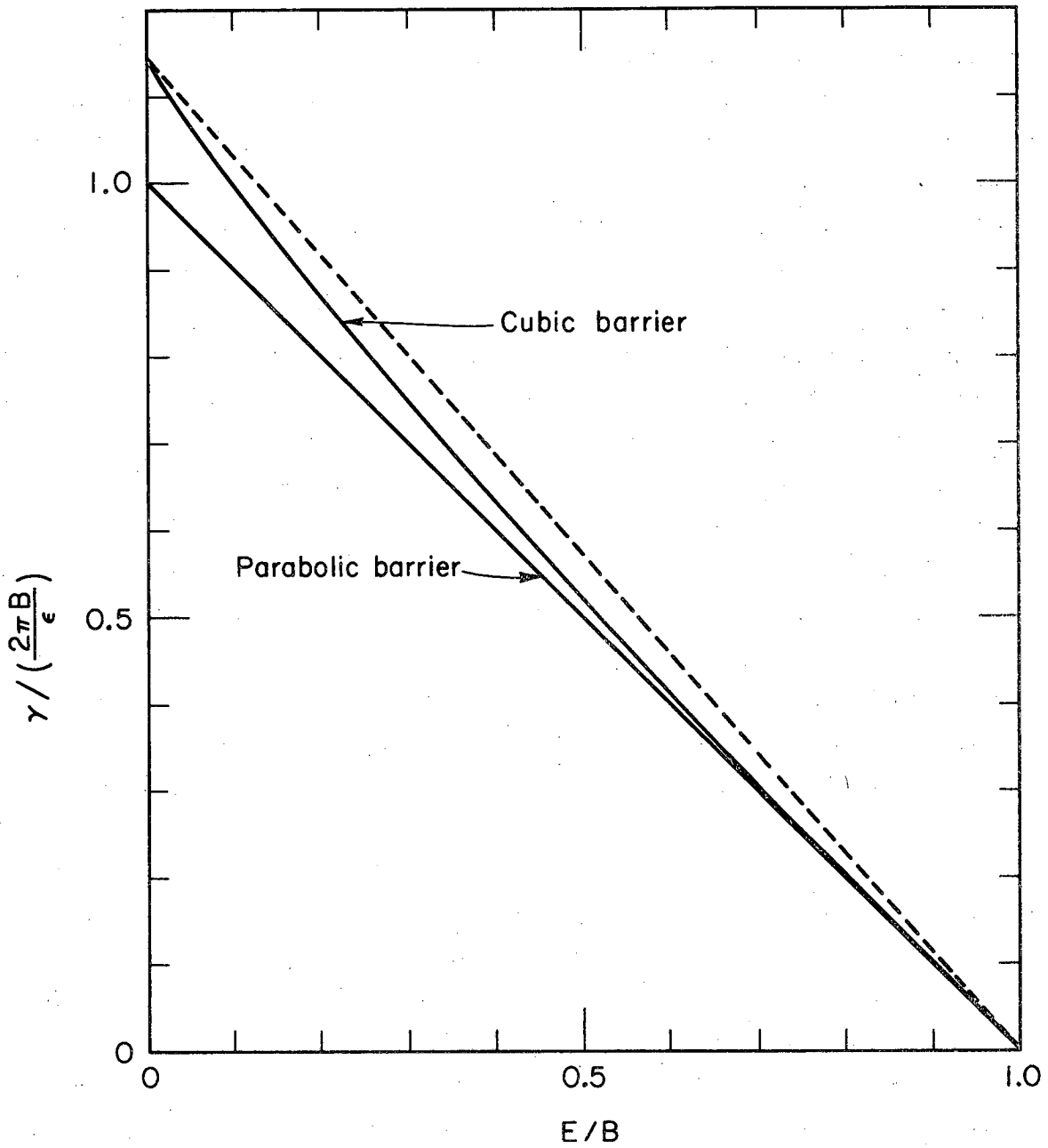

MUB-10351

Fig. 7. The penetrability exponent γ divided by $(2\pi B/\epsilon)$ as a function of the total energy E in the fission degree of freedom divided by B. The solid straight line shows the result for a parabolic barrier [Eq. (24b)]. The result for a cubic barrier as calculated from the exact equations (32) of Appendix B is given by the solid curved line; the simple approximate equation (29) yields a result that cannot be distinguished on a graph of this scale from the one shown. The dashed straight line shows the approximate result for a cubic barrier obtained by neglecting the logarithmic term in Eq. (29).

general the fission coordinate is not uncoupled from the nonfission coordinates, and consequently the solution of the coupled multidimensional barrier-penetration problem represents a question of central importance in fission theory and should be studied in detail.

The above formalism for fission widths has been used to deduce values of ϵ for a variety of nuclei from the available experimental data on fission probabilities. (Appropriate analyses made in conjunction with the original experiments are reproduced verbatim. This includes any corrections for the effects of finite counter resolution; except where originally made the data have not been corrected for such effects.) The assumption is made in each case that the transition-state levels are widely separated so that only the lowest level contributes, although in practice this is not always a good assumption. The deduced values of $\epsilon = |\hbar\omega_2|$ are converted from MeV to natural liquid-drop units by use of Eq. (21), and the fissility parameters corresponding to the various nuclei are determined from Eq. (20). The experimental values obtained in this way are compared in Fig. 8 with the calculated dependence of $|\omega_2|$ on x.

We shall now summarize the various types of experimental measurements used to accumulate the data of Fig. 8. For a nucleus whose fission barrier is larger than its neutron binding energy, ϵ can be determined directly from Eq. (25) by measuring the average fission width $\Gamma_f(E^*)$ and the average level spacing $D(E^*) = 1/\rho(E^*)$ at slow-neutron energies and determining the combination $B + X_L - \frac{1}{2}\hbar\omega_{gs}$ from an analysis of the fission cross-section curve at higher neutron energies (32,33).

From measured values for the spontaneous-fission lifetime [equal to $\hbar$ divided by $\Gamma_f(0)$] and the combination $B - \frac{1}{2}\hbar\omega_{gs}$ the quantity ϵ can be found from Eq. (30), provided that an independent estimate of $\hbar\omega_{gs}$ is available [see for example Eq. (28)]. We have used the data of Refs. (31) and (33).

The measurement of the slope of the fission cross-section curve at $E^* = B + X_L - \frac{1}{2}\hbar\omega_{gs}$ can be used for a nucleus whose barrier height is less than or not much larger than its neutron binding energy so that neutron emission can be neglected. The fission cross section $\sigma_f(E^*)$ can be written as

$$\sigma_f(E^*) = \sigma_r(E^*)\ \Gamma_f(E^*)/\Gamma_t(E^*) \quad , \tag{31}$$

where $\sigma_r(E^*)$ is the total reaction cross section and $\Gamma_t(E^*)$ is the total decay width, which consists principally of the width for electromagnetic de-excitation. If the reasonable assumption is made that $\Gamma_f(E^*)$ varies more rapidly with the excitation energy E^* than either $\sigma_r(E^*)$ or $\Gamma_t(E^*)$ and that the exponential term in $\Gamma_f(E^*)$ varies more rapidly than the level density $\rho(E^*)$, then it follows from Eqs. (25) and (31) that

$$\frac{d\sigma_f(B + X_L - \frac{1}{2}\hbar\omega_{gs})}{dE^*} \approx \frac{\pi}{2}\,\frac{\sigma_f^{plat}}{\epsilon} \quad ,$$

where σ_f^{plat} is the value of $\sigma_f(E^*)$ at the plateau corresponding to fission through the lowest level. This method is used to analyze data both for neutron-induced fission (34,35) and for the (d,pf) reaction (36).

For nuclei in which fission cross-section measurements have been made at energies somewhat below the top of the fission barrier, as for example in photofission (37), ϵ can be deduced by measuring the logarithmic slope of the fission cross-section curve. The same arguments as above applied to Eqs. (26) and (31) lead to

$$\frac{d \log \sigma_f}{dE^*} \approx \frac{2\pi \log e}{\epsilon} \quad , \qquad E^* < B + X_L - \tfrac{1}{2}\hbar\omega_{gs} \quad .$$

We consider finally the case of a nucleus whose fission barrier is much larger than its neutron binding energy. For excitation energies comparable to the barrier height the total decay width $\Gamma_t(E^*)$ is then primarily the width $\Gamma_n(E^*)$ for the emission of neutrons. Therefore provided $\sigma_r(E^*)$ is known, the ratio $\Gamma_f(E^*)/\Gamma_n(E^*)$ can be determined from Eq. (31) by measuring the fission cross section $\sigma_f(E^*)$. The dependence of $\Gamma_f(E^*)/\Gamma_n(E^*)$ on E^* can then be analyzed to yield an estimate of ϵ. This procedure is followed in Refs. (38) and (39), where a conventional expression is used for $\Gamma_n(E^*)$ and where $\Gamma_f(E^*)$ is calculated according to Eqs. (22), (23) and (24); the transition-state energy levels X_i are assumed to be distributed according to a Fermi-gas level-density formula.

In connection with our above discussion it should be pointed out that what is customarily determined experimentally from fission cross-section measurements and referred to as the barrier height is <u>not</u> the true height of

Fig. 8. A comparison of the calculated and experimental values of the magnitude of the purely imaginary frequency ω_2 that is relevant for penetration of the fission barrier, as a function of the fissility parameter x. In converting the experimental values of $\epsilon = |\hbar\omega_2|$ from MeV to the natural liquid-drop units of $[E_s^{(0)}/(M_0R_0^2)]^{\frac{1}{2}}$ the values of Myers and Swiatecki (6) have been used for the constants of the semiempirical mass formula [see Eqs. (20) and (21)]. No arbitrary parameters have been adjusted; the calculated curve has not been normalized to the experimental points in any way. The portion of the calculated curve indicated by the dashed line is of questionable accuracy. The data are as follows (arrows pointing downward denote upper limits):

○ Leonard and Odegaarden (32), slow-neutron fission widths;

□ Bowman and Hoff (33), slow-neutron fission widths;

▽ Bowman and Hoff (33), spontaneous-fission lifetimes;

△ Viola and Wilkins (31), spontaneous-fission lifetimes;

● Leonard (34), slopes of σ_f vs E^* at $E^* = B + X_L - \frac{1}{2}\hbar\omega_{gs}$ for neutron-induced fission;

▼ Henkel (35), slopes of σ_f vs E^* at $E^* = B + X_L - \frac{1}{2}\hbar\omega_{gs}$ for neutron-induced fission;

■ Northrop et al. (36), slopes of σ_f vs E^* at $E^* = B + X_L - \frac{1}{2}\hbar\omega_{gs}$ for (d,pf) reactions;

▲ Katz et al. (37), slopes of log σ_f vs E^* at E^* somewhat less than $B + X_L - \frac{1}{2}\hbar\omega_{gs}$ for photofission;

Tall error bars with no symbol, Khodai-Joopari (39), analysis of σ_f vs E^* for proton- and alpha-induced fission.

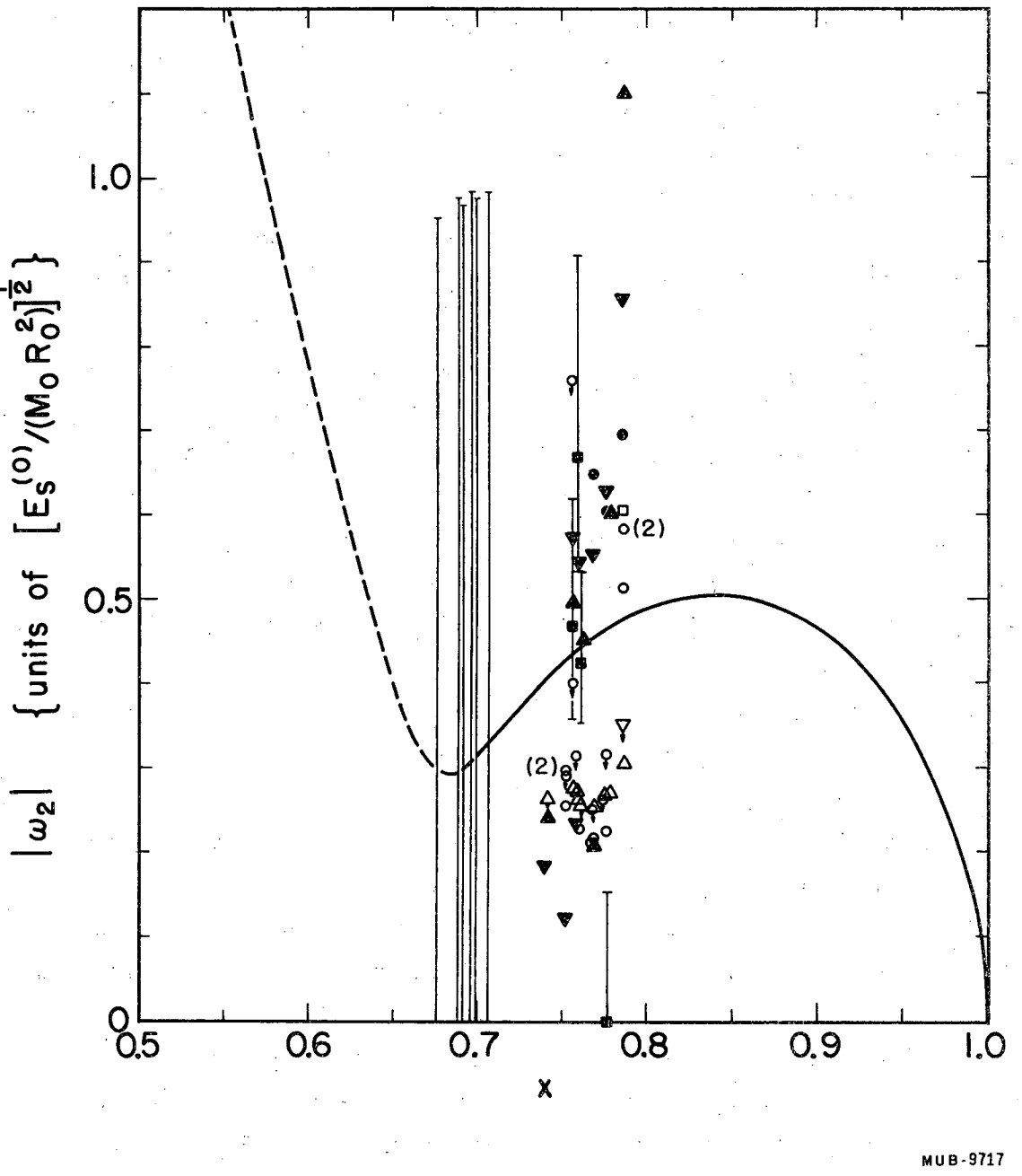

MUB-9717

Fig. 8.

the barrier. Insofar as the assumption that the fission coordinate is uncoupled from the other coordinates is valid the experimentally determined quantity is the barrier height B plus the energy X_L of the lowest state at the saddle point for the nonfission degrees of freedom having the appropriate quantum numbers minus the zero-point energy $\frac{1}{2}\hbar\omega_{gs}$ in the fission degree of freedom, i.e. the combination $B + X_L - \frac{1}{2}\hbar\omega_{gs}$ that appears in our formulae. (In the general case of a coupled system the experimentally determined quantity is this combination minus the sum of the zero-point energies in the nonfission degrees of freedom at the ground state plus their sum at the saddle point.) In addition we should mention that the combination $B + X_L - \frac{1}{2}\hbar\omega_{gs}$ is also very frequently referred to as the fission "threshold." However, we prefer to use this word only in its strict meaning to denote the minimum amount of energy that must be supplied for a reaction to be possible energetically. Thus for the normal fission process the threshold is a negative quantity whose magnitude equals the energy release.

It should be emphasized that once a particular set of constants has been selected for the semiempirical mass formula [in our case the set of Myers and Swiatecki (6)] there remain no adjustable parameters in the analysis. Thus the calculated curve of Fig. 8 has not been normalized to the experimental data in any way.

The uncertainties in most of the experimental values of ϵ are very large, and the data are unfortunately not sufficiently accurate to provide a sensitive test of the theory. For example it is seen that for a given nucleus the values of ϵ obtained by different methods (and in some cases even by the same method) differ widely from one another. At least one regularity can nevertheless be observed in the data: the values obtained from the measured spontaneous-fission lifetimes are approximately the same for all nuclei.

The general impression one gets from the comparison is that the theory does give the correct order of magnitude of ϵ. It is hoped that the accuracy of future experimental determinations will be increased to the point where this can be confirmed and the details of the theory can be tested. In particular it would be of interest to determine ϵ experimentally for some very light nuclei, for which, as discussed in Subsection III.B, this quantity is predicted to be exceptionally large.

V. SUMMARY AND CONCLUSION

We have attempted the first step in a systematic discussion of the dynamics of the fission process—the study of the normal modes of oscillation of an idealized uniformly charged drop about its saddle-point shape. For axially symmetric drops we have presented the frequencies and eigenvectors of the normal modes as functions of the fissility parameter for the range $0.7 \leq x \leq 1.0$ and also, with questionable accuracy, the frequencies of the symmetric modes for $0.3 \leq x < 0.7$.

We have indicated how the information regarding the normal modes can be used to discuss (1) certain aspects of the transition-state spectrum, (2) the probability of finding the system in a given state of motion when it is in the neighborhood of the saddle point and (3) the penetration of the fission barrier. Comparisons between the theory and experimental data were possible only as regards the third item. It was seen that the calculations are capable of reproducing the correct order of magnitude of the frequency ω_2 for motion in the fission direction but that the data are not sufficiently accurate to permit a more definitive conclusion at this time.

There is need for more experimental work on both the first and the third items. In particular the identities and energies of the saddle-point quantum states should be determined, and $\epsilon = |\hbar\omega_2|$ should be measured with greatly increased precision and over a wider range of the fissility parameter, especially for very small values of x.

Further theoretical work on all three items should be performed. In connection with the first, the energies of the non-axially symmetric collective vibrations, rotational states and single-particle excitations should be worked out. In connection with the third, barrier penetration for a multidimensional system in which the fission coordinate is not assumed uncoupled from the nonfission coordinates should be studied. But to us the major outstanding theoretical problem is related to the second item. If our basic understanding of the fission process is to progress theoretically, it is now necessary to perform for the heavier elements the dynamical calculations that provide the relationship between the initial states of motion near the saddle point and the final states of motion of the fragments at infinity. This would transform the predicted probability distributions for the initial states of motion into probability distributions

for such observable properties of fission fragments as their division of mass, translational kinetic energies and excitation energies. A direct comparison without the use of adjustable parameters could then be made with the large amount of existing data on the fission of elements heavier than radium, and in this way the applicability of the liquid-drop model for discussing fission could be more reliably ascertained.

ACKNOWLEDGMENTS

It is a pleasure to acknowledge the hospitality of the Niels Bohr Institute, Copenhagen, Denmark, where much of this work was performed under the financial support of a NATO Postdoctoral Fellowship in Science. The remainder was completed at the Lawrence Radiation Laboratory under the support of the U. S. Atomic Energy Commission. Stimulating discussions concerning this work were held with various members and guests of both institutes. I wish to thank in particular at the Niels Bohr Institute Sven Bjørnholm, Cho Yi-chung and Richard K. Cooper and at the Lawrence Radiation Laboratory Shyam S. Kapoor, William D. Myers, John O. Rasmussen, Stanley G. Thompson and especially Wladyslaw J. Swiatecki, who contributed many of the ideas discussed here.

I am grateful to Stanley Cohen and Wladyslaw J. Swiatecki for permission to use the unpublished results of their calculations of the stiffness matrix and to Frank Plasil for calculating with their code more accurate values than were previously available. I would also like to thank John H. Gunn for his instruction and advice on coding in ALGOL and the Astronomical Observatory of the University of Copenhagen for the use of its GIER computer, on which the numerical calculations were performed.

APPENDICES

A. The Convergence of the Calculations as a Function of L and N

The accuracy of the calculated liquid-drop frequencies and eigenvectors is limited by two factors: (1) the accuracy with which the stiffness and inertia matrices can be calculated and (2) how well the solution of the reduced matrix problem [Eq. (15)] in N dimensions represents the solution of the complete infinite-dimensional problem. We will discuss each of these factors in turn.

The accuracy of K and M is limited by the precision with which saddle-point shapes are known. As discussed in Ref. (8) saddle-point shapes are determined in a Legendre-polynomial parametrization very accurately for the range $0.7 \leq x \leq 1.0$, moderately accurately for $0.5 \leq x < 0.7$, and with uncertain accuracy, at least in some respects, for $0.3 \leq x < 0.5$. Thus the specification of the saddle-point shapes for $x < 0.7$ introduces an inherent limitation on the accuracy of K and M and consequently of the frequencies and eigenvectors for this range of x.

Since K is the matrix of second partial derivatives of the potential energy evaluated at the saddle point its accuracy is restricted only by the precision with which second derivatives can be determined numerically (see again the discussion in Subsection II.B.2). On the other hand, the accuracy of M is intrinsically limited by how well the velocity potential φ can be approximated by a finite number L of terms in an expansion such as (9). For $x = 0.7$ a study was made of the convergence as a function of L of the calculated inertia matrix and of the final calculated frequencies, eigenvectors and normal-coordinate stiffness and inertia constants. The results for the frequencies are shown in Fig. 9. It is observed that in general the symmetric frequencies converge more rapidly than the asymmetric ones and that the lower frequencies converge more rapidly than the higher ones. One can conclude from Fig. 9 that for a given ω_n the calculations have converged sufficiently at a value of L that is somewhat larger than n. Analogous results were obtained for the convergence of the other quantities with L but will not be given here.

A similar study was made for $x = 0.7$ of how well the solution of the reduced matrix problem [Eq. (15)] in a small number of dimensions can be expected to represent the solution of the complete infinite-dimensional

problem. Equation (15) was reduced to a smaller number of dimensions by systematically eliminating rows and columns of K and M; the frequencies, eigenvectors and normal-coordinate stiffness and inertia constants were then calculated from the resulting reduced equations. Figure 10 contains the results for the frequencies. As would be expected from the variational principle the squares of the frequencies essentially decrease monotonically with increasing N. In addition we observe that the lower frequencies converge more rapidly than the higher ones and that the 10 lowest frequencies appear to have converged sufficiently for N = 18. Analogous results were obtained for the convergence of the other quantities with N but will not be given here.

The convergence of the calculations with respect to both L and N improves progressively as x is increased from 0.7 to 1.0. We can therefore conclude that for the range $0.7 \leq x \leq 1.0$, where the saddle-point shapes are accurately determined in a Legendre-polynomial parametrization, the calculations converge as well as or better than the ones discussed here for $x = 0.7$. Hence the detailed results for the 8 lowest modes presented in Table I (and consequently the results represented by the solid lines in Figs. 1-4 and 8 and the results of Figs. 5a and 5b) are essentially free of errors arising from the lack of convergence in either L or N.

On the other hand, for $x < 0.7$ there are several sources of error, and for this region we make no guarantee of the accuracy of the results reported for the symmetric frequencies. However, we see in Figs. 1 and 2 that for the range $0.3 \leq x \leq 0.5$ there is reasonable agreement between the present results for ω_4 and those calculated on the basis of a two-spheroid parametrization of fission shapes. This leads one to believe that the present calculations may be moderately accurate with regard to the symmetric frequencies even for small values of x.

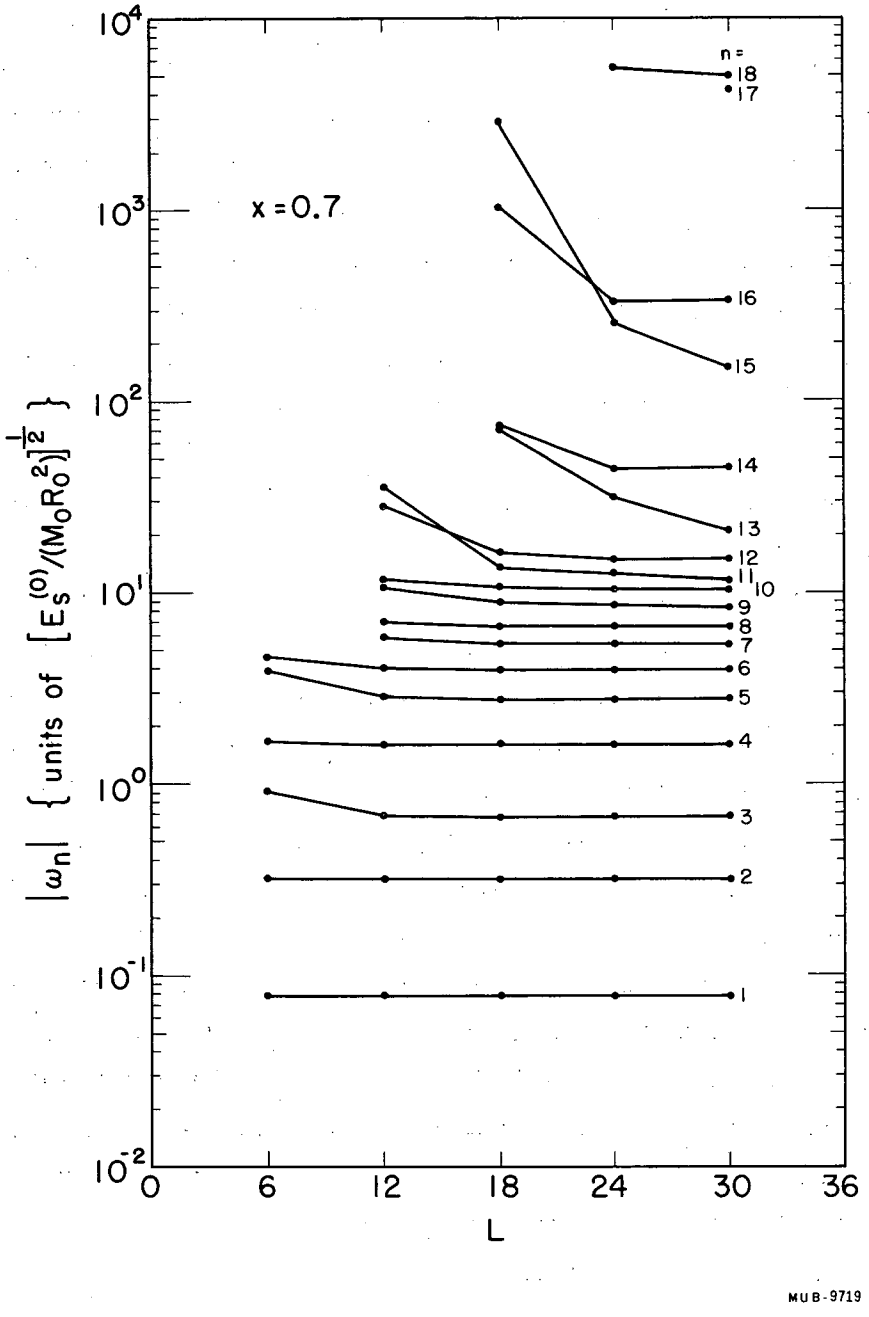

Fig. 9. The convergence of the calculated magnitudes of the frequencies as a function of L for x = 0.7. The quantity L gives the number of terms retained in the expansion of the velocity potential φ [Eq. (9)].

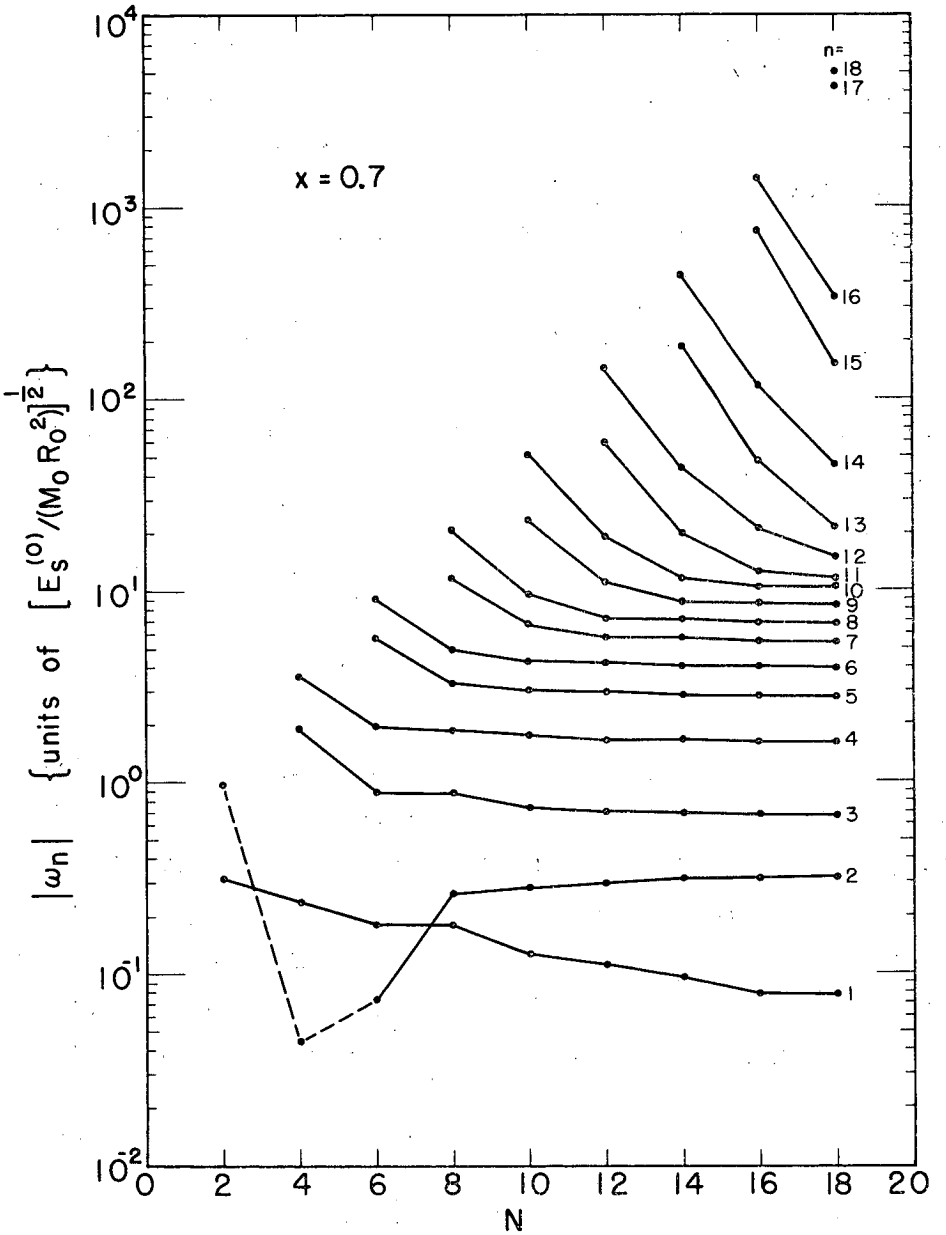

Fig. 10. The convergence of the calculated magnitudes of the frequencies as a function of N for x = 0.7. The dimensions of the determinantal equations solved for the symmetric frequencies and for the asymmetric frequencies are each N/2. The dashed line indicates that the sign of ω_2^2 has changed; ω_2^2 is negative for $N \geq 6$ whereas it is positive for $N \leq 4$. Thus the dependence of ω_2^2 on N is qualitatively the same as the dependences on N of the remaining squares of the frequencies.

B. The Penetrability of a Cubic Barrier

We consider a one-dimensional cubic potential-energy barrier $V(\beta)$ defined relative to its local minimum, which is located at $\beta = 0$. The height of the barrier is taken as B and the second derivative at its top as the negative quantity K_2; this implies definite values for the coefficients of the quadratic and cubic terms. The equation for our barrier is therefore

$$V(\beta) = \tfrac{1}{2}\,|K_2|\beta^2 - \tfrac{1}{3}[|K_2|^3/(6B)]^{\frac{1}{2}}\beta^3 \quad .$$

The deformation coordinate β is related to the normal coordinate β_2 of the text, which is defined relative to the saddle point, by

$$\beta = \beta_2 + \hat{\beta} \quad ,$$

where

$$\hat{\beta} = (6B/|K_2|)^{\frac{1}{2}}$$

is the value of β corresponding to the top of the barrier. The effective mass M_2 for motion in the fission direction is assumed to be independent of β. (The present results also apply to the case in which M_2 is not constant but for which the dependence on β of the product of M_2 and $V - E$ is cubic.)

The penetrability P is calculated as a function of the energy E in the fission degree of freedom (relative to the barrier's local minimum; see the diagram in Fig. 6). In the WKB approximation the penetrability is given by (40)

$$P = \frac{1}{1 + \exp[\gamma(E)]} \quad ,$$

where for $0 \leq E \leq B$ the exponent is

$$\gamma(E) = \frac{2(2M_2)^{\frac{1}{2}}}{\hbar} \int_{\beta_1}^{\beta_2} [V(\beta) - E]^{\frac{1}{2}}\, d\beta \quad .$$

The limits of integration β_1 and β_2 are the two appropriate zeros of the integrand.

We denote respectively by K(k) and E(k) the complete elliptic integrals of the first and second kinds. [No confusion should arise over our use of the symbols E for the energy and E(k) for an elliptic integral.] In terms of these functions the above integral for $\gamma(E)$ can be expressed as

$$\gamma(E) = \frac{36B}{5\epsilon}\left\{[\cos\varphi + (3)^{-\frac{1}{2}}\sin\varphi]^{\frac{1}{2}}\,E(k) - \frac{[2(E/B) - 1 + \cos\varphi + (3)^{\frac{1}{2}}\sin\varphi]}{3[\cos\varphi + (3)^{-\frac{1}{2}}\sin\varphi]^{\frac{1}{2}}}\,K(k)\right\} , \tag{32a}$$

where

$$\varphi = \frac{1}{3}\arccos[1 - 2(E/B)] \tag{32b}$$

and

$$k^2 = \frac{1 - (3)^{-\frac{1}{2}}\tan\varphi}{1 + (3)^{-\frac{1}{2}}\tan\varphi} . \tag{32c}$$

The quantity ϵ has the same definition here as in the text:

$$\epsilon = |\hbar\omega_2| = \hbar(|K_2|/M_2)^{\frac{1}{2}} .$$

There are two limiting cases in which the result for $\gamma(E)$ simplifies. When the energy is near the bottom of the barrier we find

$$\gamma(E) \approx \frac{36B}{5\epsilon}\left\{1 - \frac{5}{36}\left[1 + 4\ln 2 + 3\ln 3 + \ln\left(\frac{B}{E}\right)\right]\frac{E}{B}\right\}$$

$$\approx \frac{36}{5\epsilon}\left\{B - \left[0.98173 + 0.13889\ln\left(\frac{B}{E}\right)\right]E\right\} , \qquad \frac{E}{B} \ll 1 .$$

Second, when the energy is near the top of the barrier the barrier shape is approximately parabolic, and, as would be expected, Eqs. (32) simplify to the exact result for a parabolic barrier, which is

$$\gamma(E) \approx \frac{2\pi B}{\epsilon}\left(1 - \frac{E}{B}\right) , \qquad 1 - \frac{E}{B} \ll 1 .$$

By considering these two limiting forms we have arrived at a simple but yet accurate expression for $\gamma(E)$ that is valid for all values of E from the bottom to the top of the barrier, viz.

$$\gamma(E) \approx \frac{36}{5\epsilon}\left\{B - \left[1 + \left(1 - \frac{2\pi}{36/5}\right) \ln\left(\frac{B}{E}\right)\right] E\right\}$$

$$\approx \frac{36}{5\epsilon}\left\{B - \left[1 + 0.12734 \ \ln\left(\frac{B}{E}\right)\right] E\right\} \quad , \qquad 0 \leq \frac{E}{B} \leq 1 \quad .$$

Over the entire range of E from 0 to B the values of $\gamma/\left(\frac{2\pi B}{\epsilon}\right)$, i.e. the quantity plotted in Fig. 7, calculated from this equation differ from the exact results of Eqs. (32) by less than 0.002. In addition this approximate formula reproduces correctly the exact values and first derivatives of $\gamma(E)$ at both E = 0 and E = B.

REFERENCES

1. David Lawrence Hill and John Archibald Wheeler, Nuclear Constitution and the Interpretation of Fission Phenomena, Phys. Rev. 89, 1102 (1953).
2. U. L. Businaro and S. Gallone, On the Interpretation of Fission Asymmetry According to the Liquid Drop Nuclear Model, Nuovo Cimento 1, 629 (1955).
3. James Rayford Nix and Wladyslaw J. Swiatecki, Studies in the Liquid-Drop Theory of Nuclear Fission, Nucl. Phys. 71, 1 (1965). James Rayford Nix, Studies in the Liquid-Drop Theory of Nuclear Fission (Ph. D. Thesis), University of California Lawrence Radiation Laboratory Report UCRL-11338, April 1, 1964 (unpublished).
4. Lawrence Wilets, Theories of Nuclear Fission (Clarendon Press, Oxford, 1964), Chap. 3, Subsec. 4.2, "Barrier Penetration," pp. 50-53.
5. J. J. Griffin, Transition States at the Fission Barrier, Paper No. SM-60/4, in Physics and Chemistry of Fission, Proceedings of a Symposium held in Salzburg, 1965, Vol. I (International Atomic Energy Agency, Vienna, 1965), p. 23.
6. William D. Myers and Wladyslaw J. Swiatecki, Nuclear Masses and Deformations, University of California Lawrence Radiation Laboratory Report UCRL-11980, May 27, 1965, to be published in Nucl. Phys.
7. W. J. Swiatecki, Deformation Energy of a Charged Drop. II. Symmetric Saddle Point Shapes, Phys. Rev. 104, 993 (1956).
8. Stanley Cohen and Wladyslaw J. Swiatecki, The Deformation Energy of a Charged Drop, Part V: Results of Electronic Computer Studies, Ann. Phys. (N. Y.) 22, 406 (1963).
9. Horace Lamb, Hydrodynamics, 6th ed. (Dover Publications, New York, 1945), Sec. 9, pp. 6-8.
10. Herbert Goldstein, Classical Mechanics (Addison-Wesley Publishing Company, Inc., Reading, Mass., 1959), Chap. 1, Sec. 6, "Simple applications of the Lagrangian formulation," pp. 22, 23.
11. Niels Bohr and John Archibald Wheeler, The Mechanism of Nuclear Fission, Phys. Rev. 56, 426 (1939).
12. Wladyslaw J. Swiatecki, Deformation Energy of a Charged Drop, III. Further Developments, Paper No. P/651, in Proceedings of the Second United Nations International Conference on the Peaceful Uses of Atomic Energy, held in Geneva, 1958, Vol. 15, Physics in Nuclear Energy (United Nations, Geneva, 1958), p. 248.

13. Stanley Cohen and W. J. Swiatecki, The Deformation Energy of a Charged Drop, IV. Evidence for a Discontinuity in the Conventional Family of Saddle Point Shapes, Ann. Phys. (N. Y.) 19, 67 (1962).

14. A. R. Edmonds, Angular Momentum in Quantum Mechanics (Princeton University Press, Princeton, New Jersey, 1957), Chap. 3, Sec. 7, "The Wigner 3-j Symbol," pp. 45-50; Chap. 4, Sec. 6, "Integrals Involving the $\mathcal{D}^{(j)}_{m'm}(\alpha\ \beta\ \gamma)$," pp. 62, 63.

15. W. D. Foland and R. D. Present, Hydrodynamic Theory of Spontaneous Fission, Phys. Rev. 113, 613 (1959).

16. S. Frankel and N. Metropolis, Calculations in the Liquid-Drop Model of Fission, Phys. Rev. 72, 914 (1947).

17. Granino A. Korn and Theresa M. Korn, Mathematical Handbook for Scientists and Engineers (McGraw-Hill Book Company, Inc., New York, 1961), Chap. 20, Sec. 8-4, "Approximation-function Methods for Numerical Solution of Boundary-value Problems," pp. 678, 679.

18. Philip Davis and Philip Rabinowitz, Additional Abscissas and Weights for Gaussian Quadratures of High Order: Values for n=64, 80, and 96, J. Research NBS 60, 613 (1958).

19. V. G. Nossoff, On the Theory of Nuclear Fission Near Threshold, Paper No. P/653, in Proceedings of the International Conference on the Peaceful Uses of Atomic Energy, held in Geneva, 1955, Vol. 2, Physics; Research Reactors (United Nations, New York, 1956), p. 205.

20. Herbert Goldstein, Classical Mechanics (Addison-Wesley Publishing Company, Inc., Reading, Mass., 1959), Chap. 10, "Small Oscillations," pp. 318-346.

21. Alex E. S. Green, Nuclear Physics (McGraw-Hill Book Company, Inc., New York, 1955), pp. 185, 250.

22. John William Strutt, Baron Rayleigh, The Theory of Sound, Vol. II (Dover Publications, New York, 1945), Sec. 304, Eq. (1), p. 172; Sec. 306, Eq. (6), p. 178.

23. Aage Bohr, On the Theory of Nuclear Fission, Paper No. P/911, in Proceedings of the International Conference on the Peaceful Uses of Atomic Energy, held in Geneva, 1955, Vol. 2, Physics; Research Reactors (United Nations, New York, 1956), p. 151.

24. E. Wigner, The Transition State Method, Trans. Faraday Soc. 34, part 1, 29 (1938).

25. J. R. Huizenga, J. P. Unik and B. D. Wilkins, On the Role of the Transition State Nucleus in Fission, Paper No. SM-60/3, in Physics and Chemistry of Fission, Proceedings of a Symposium held in Salzburg, 1965, Vol. I (International Atomic Energy Agency, Vienna, 1965), p. 11.

26. Samuel Glasstone, Keith J. Laidler, and Henry Eyring, The Theory of Rate Processes (McGraw-Hill Book Company, Inc., New York, 1941), Chap. III, "Potential-energy Surfaces," Chap. IV, "Statistical Treatment of Reaction Rates," pp. 85-201.

27. L. D. Landau and E. M. Lifshitz, Statistical Physics, translated by E. Peierls and R. F. Peierls (Addison-Wesley Publishing Company, Inc., Reading, Mass., 1958), Sec. 30, "The probability distribution for an oscillator," pp. 86-89.

28. Albert Messiah, Quantum Mechanics, Vol. I, translated by G. M. Temmer (Interscience Publishers, New York, 1961), Chap. XII, Sec. 12, "Harmonic Oscillators in Thermodynamic Equilibrium," pp. 448-451.

29. John A. Wheeler, Channel Analysis of Fission, in Fast Neutron Physics, Part II: Experiments and Theory, edited by J. B. Marion and J. L. Fowler (Interscience Publishers, New York, 1963), p. 2051.

30. L. D. Landau and E. M. Lifshitz, Quantum Mechanics, Non-Relativistic Theory, translated by J. B. Sykes and J. S. Bell (Addison-Wesley Publishing Company, Inc., Reading, Mass., 1958), Sec. 50, "Penetration through a potential barrier," pp. 171-178.

31. V. E. Viola, Jr. and B. D. Wilkins, Fission Barriers and Half-Lives of the Trans-Radium Elements, Argonne National Laboratory, preprint (no date), submitted for publication to Nucl. Phys.

32. B. R. Leonard, Jr. and R. H. Odegaarden, Subthreshold Fission - U^{236}, U^{238}, Pu^{240}, Pu^{242}, Pa^{231}, in Nuclear Physics Research Quarterly Report, July, August, September, 1960, Hanford Atomic Products Operation Report HW-67219, October 20, 1960, p. 4 (unpublished).

33. C. D. Bowman and R. W. Hoff, The Spontaneous Fission Half-Life of Am^{242M} and the Shape of the Fission Barrier for Am^{242}, University of California Lawrence Radiation Laboratory, Livermore, preprint (no date).

34. B. R. Leonard, Jr., Subthreshold Fission, in Nuclear Physics Research Quarterly Report, October, November, December, 1958, Hanford Atomic Products Operation Report HW-59126, January 20, 1959, p. 3 (unpublished).

35. R. L. Henkel, Fission by Fast Neutrons, in Fast Neutron Physics, Part II: Experiments and Theory, edited by J. B. Marion and J. L. Fowler (Interscience Publishers, New York, 1963), p. 2001.

36. John A. Northrop, Richard H. Stokes, and Keith Boyer, Measurement of the Fission Thresholds of Pu^{239}, U^{233}, U^{235}, and U^{238} Using the (d,p) Reaction, Phys. Rev. 115, 1277 (1959).

37. L. Katz, A. P. Baerg and F. Brown, Photofission in Heavy Elements, Paper No. P/200, in Proceedings of the Second United Nations International Conference on the Peaceful Uses of Atomic Energy, held in Geneva, 1958, Vol. 15, Physics in Nuclear Energy (United Nations, Geneva, 1958), p. 188.

38. Donald S. Burnett, Raymond C. Gatti, Franz Plasil, P. Buford Price, Wladyslaw J. Swiatecki, and Stanley G. Thompson, Fission Barrier of Thallium-201, Phys. Rev. 134, B952 (1964).

39. Arastoo Khodai-Joopari, Fission Properties of Some Elements Below Radium (Ph. D. Thesis), University of California Lawrence Radiation Laboratory Report UCRL-16489 (unpublished).

40. Nanny Fröman and Per Olof Fröman, JWKB Approximation (North-Holland Publishing Company, Amsterdam, 1965), Chap. 9, Sec. 1, "Barrier penetration when the kinetic energy of the incident particle lies below the energy corresponding to the top of the barrier," pp. 92-97.

This report was prepared as an account of Government sponsored work. Neither the United States, nor the Commission, nor any person acting on behalf of the Commission:

A. Makes any warranty or representation, expressed or implied, with respect to the accuracy, completeness, or usefulness of the information contained in this report, or that the use of any information, apparatus, method, or process disclosed in this report may not infringe privately owned rights; or

B. Assumes any liabilities with respect to the use of, or for damages resulting from the use of any information, apparatus, method, or process disclosed in this report.

As used in the above, "person acting on behalf of the Commission" includes any employee or contractor of the Commission, or employee of such contractor, to the extent that such employee or contractor of the Commission, or employee of such contractor prepares, disseminates, or provides access to, any information pursuant to his employment or contract with the Commission, or his employment with such contractor.